https://doi.org/10.5194/egusphere-2026-721
Preprint. Discussion started: 10 March 2026
© Author(s) 2026. CC BY 4.0 License.

Historical and Projected Changes in Temperature–Precipitation Compound Hot and Dry Extremes across Africa Based on CMIP5 and CMIP6 Ensemble Simulations

Paul Adigun [1]; Koji Dairaku [1]; Akinwale T. Ogunrinde [2,*]; Ebiendele Precious [1]; Muhammad Umar Nadeem [1]; Ermias Sisay Brhane [1]; Xian Xue [2]

[1] *Department of Engineering Mechanics and Energy, University of Tsukuba, 3F300 Tennodai 1-1-1, Tsukuba, 305-8573, Japan.*

[2] *Key Laboratory of Ecological Safety and Sustainable Development in Arid Lands, Northwest Institute of Eco-Environment and Resources, Chinese Academy of Sciences, Lanzhou, Gansu, China*

* Correspondence to: ogunrindeakinwale@nieer.ac.cn

Abstract

Compound climate extremes pose disproportionate risks to societies and ecosystems, yet their evolution across Africa remains poorly constrained. Here we present the first continent-wide, multi-generation assessment of historical and projected temperature–precipitation compound hot–dry extremes across Africa using CMIP5 and CMIP6 multi-model ensembles under the full range of emission scenarios. Observations indicate continent-wide warming of 0.21 °C decade^{-1} during 1980–2020, accompanied by spatially heterogeneous precipitation trends, establishing a baseline of increasing compound vulnerability. Despite projected increases in precipitation over much of tropical Africa, both CMIP5 and CMIP6 consistently project strong intensification of compound hot–dry extremes, driven primarily by accelerated warming. By mid-century (2035–2065), compound hot–dry frequency increases across all regions, with southern Africa experiencing 0.33–0.43 hot–dry months yr^{-1} in CMIP6. By end-century (2070–2100), frequencies in western and eastern southern Africa reach 0.36–0.62 months yr^{-1} under high-emission scenarios, representing more than a doubling relative to low-emission pathways. Compound event severity intensifies nonlinearly: cumulative event magnitude exceeds 10–13 σ in southern Africa and Madagascar, while mean event duration lengthens from ~1–1.5 months historically to 4–6 months under high emissions. CMIP6 systematically projects stronger increases in compound frequency, magnitude, and duration than CMIP5, reflecting enhanced land–atmosphere coupling and higher climate sensitivity. Although strong mitigation substantially limits these increases, compound hot–dry extremes intensify even under low-emission pathways. These results demonstrate that compound climate risk may escalate regardless of mean precipitation trends, underscoring the urgency of compound-aware adaptation strategies and the substantial mitigation benefits of limiting future climate impacts.

https://doi.org/10.5194/egusphere-2026-721
Preprint. Discussion started: 10 March 2026
© Author(s) 2026. CC BY 4.0 License.

Keywords: Compound hot-dry extremes; Africa; CMIP5; CMIP6; Climate projections; Land-atmosphere coupling

Introduction

Compound climate extremes—the simultaneous or sequential occurrence of multiple hazardous conditions—pose substantially greater risks to human and natural systems than individual extremes acting in isolation (Zscheischler et al., 2018; AghaKouchak et al., 2020). Among the most consequential compound events are concurrent hot and dry conditions, which amplify drought severity by increasing evaporative demand, accelerate vegetation stress and wildfire risk, and cascade through interconnected food-water-energy systems, with devastating socioeconomic impacts (Miralles et al., 2019; Vogel et al., 2021). While considerable progress has been made in understanding compound hot-dry extremes in mid-latitude regions, their characterization across Africa—a continent uniquely vulnerable to climate variability and change—remains critically understudied despite the profound implications for over 1.4 billion people dependent on climate-sensitive livelihoods.

Africa's exposure to compound hot-dry extremes is shaped by distinct regional climate dynamics that create pronounced vulnerability gradients across the continent. The Sahel transitions between hyper-arid northern conditions and humid equatorial influences, rendering it exceptionally sensitive to rainfall variability and temperature anomalies that can push agricultural systems beyond critical thresholds (Sultan and Gaetani, 2016; Dosio et al., 2021). Southern African regions, governed by complex interactions between the South Atlantic and Indian Ocean circulation systems, have experienced intensifying drought conditions over recent decades, with warming temperatures exacerbating moisture deficits (Archer et al., 2021; Maúre et al., 2018). East Africa's bimodal rainfall regime creates multiple windows of compound extreme vulnerability each year, while the Congo Basin, despite its humid climate, faces emerging compound stress as regional warming progresses (Ongoma and Chen, 2017; Creese and Washington, 2016). Understanding how compound hot-dry frequencies will evolve across these diverse climate zones under different emission trajectories represents a fundamental challenge for African climate adaptation planning.

Over the past century, Africa has experienced significant warming, with temperatures in many regions increasing at rates comparable to or exceeding the global average (Collins, 2011; Engelbrecht et al., 2015). Mean annual temperatures across the continent have risen by approximately 0.5°C to 2°C since the early twentieth century, with the most pronounced warming occurring in subtropical regions and during boreal summer months (Liebmann et al.,

https://doi.org/10.5194/egusphere-2026-721
Preprint. Discussion started: 10 March 2026
© Author(s) 2026. CC BY 4.0 License.

2012; Gebrechorkos et al., 2019). Precipitation patterns have exhibited even greater complexity, with some regions experiencing significant drying trends, while others show increases or no discernible long-term changes (Nicholson, 2013; Ongoma and Chen, 2017). The Sahel region witnessed devastating droughts during the 1970s and 1980s, followed by partial recovery, while East Africa has experienced increased frequency of extreme rainfall events alongside prolonged dry spells (Lyon and DeWitt, 2012; Rowell et al., 2015). These observed changes in temperature and precipitation have profound implications for African societies and ecosystems, as agricultural productivity faces mounting pressure from shifting rainfall patterns and increased heat stress (Sultan and Gaetani, 2016; Thornton et al., 2011). Water resources, already scarce in many regions, are becoming increasingly stressed as rising temperatures enhance evaporative demand while precipitation becomes more variable and unpredictable (Schewe et al., 2014; Hagemann et al., 2013). Furthermore, climate change threatens biodiversity hotspots, coastal zones, and urban centers across the continent, compounding existing developmental challenges and potentially displacing millions of people (Warszawski et al., 2014; Clement et al., 2021).

The physical mechanisms linking hot and dry conditions generate powerful positive feedbacks that intensify compound extreme impacts beyond the sum of individual hazards. Elevated temperatures increase atmospheric vapor pressure deficit, accelerating evapotranspiration and soil moisture depletion even when precipitation totals remain near normal (Berg and Sheffield, 2018; Zhou et al., 2019). Depleted soil moisture in turn reduces latent heat flux, amplifying surface warming and creating self-reinforcing cycles that can persist for months (Seneviratne et al., 2010; Hirschi et al., 2011). These land-atmosphere coupling dynamics are particularly pronounced across African savanna and semi-arid regions where vegetation is already operating near physiological limits (Martens et al., 2017). Climate model projections consistently indicate that anthropogenic warming will intensify these feedback mechanisms, yet the regional heterogeneity of compound extreme responses across African climate zones has not been systematically evaluated across multiple model generations and emission scenarios.

The Coupled Model Intercomparison Project has evolved substantially between its fifth and sixth phases, with implications for compound extreme projections that remain largely unexplored for African regions. CMIP6 models incorporate improved representations of land-atmosphere interactions, more sophisticated vegetation dynamics, and higher spatial resolution, which should better capture the regional processes governing the occurrence of compound extremes (Eyring et al., 2016; Meehl et al., 2020). Furthermore, the transition from Representative Concentration Pathways (RCPs) to Shared Socioeconomic Pathways (SSPs) provides updated emission

https://doi.org/10.5194/egusphere-2026-721
Preprint. Discussion started: 10 March 2026
© Author(s) 2026. CC BY 4.0 License.

trajectories that reflect current understanding of socioeconomic development pathways and their associated radiative forcing (O'Neill et al., 2016; Riahi et al., 2017). Whether these modeling advances translate into meaningfully different compound extreme projections for Africa, and whether CMIP5 and CMIP6 ensembles provide consistent or divergent risk assessments, have direct implications for climate adaptation investments predicated on projected hazard frequencies.

Previous investigations of African drought and heat extremes have predominantly examined temperature and precipitation changes in isolation, overlooking the compound nature of climate risks that matter most for impact assessment (e.g. Engelbrecht et al., 2015; Almazroui et al., 2020). Studies that have addressed compound extremes globally often lack the regional granularity required for African climate adaptation planning, while regionally focused analyses have typically employed single model generations or limited scenario comparisons (e.g. Vogel et al., 2021; Manning et al., 2019; Zscheischler et al., 2020). The absence of comprehensive, multi-generation, multi-scenario assessments of compound hot-dry extreme evolution across IPCC-defined African reference regions represents a critical knowledge gap at a time when African nations are developing National Adaptation Plans and nationally determined contributions that require robust hazard projections.

This study presents the first systematic analysis of compound hot-dry extreme-frequency changes across Africa using both the CMIP5 and CMIP6 multi-model ensemble means, spanning the full range of emission scenarios from strong mitigation to high-warming pathways. Employing month-stratified percentile thresholds following the established compound extreme methodology (Manning et al., 2019), we quantify compound hot-dry month frequencies across eight IPCC-defined African reference regions for the historical baseline (1980–2020), mid-century (2035–2065), and late-century (2071–2100) periods. Our analysis addresses four key objectives: (i) characterizing the spatial patterns of projected compound hot-dry frequency across Africa under each emission scenario; (ii) evaluating the scenario dependence of compound extreme intensification across regional climate zones; (iii) comparing CMIP5 and CMIP6 projections to assess inter-generational consistency and identify regions where model advances alter risk assessments; and (iv) identifying regional hotspots where compound extreme frequencies are projected to increase most significantly, informing prioritization of adaptation resources. By providing the first comprehensive multi-model, multi-scenario assessment of African compound hot-dry extremes, this study delivers decision-relevant information for climate adaptation planning while advancing fundamental understanding of compound climate risk evolution under anthropogenic forcing.

https://doi.org/10.5194/egusphere-2026-721
Preprint. Discussion started: 10 March 2026
© Author(s) 2026. CC BY 4.0 License.

2. Data and Methods

2.1 Study Area and Regional Framework

This study encompasses the entire African continent and is analysed using the Intergovernmental Panel on Climate Change (IPCC) Sixth Assessment Report (AR6) reference regions framework (Iturbide et al., 2020). Eight climatologically coherent African subregions are examined: the Sahara (SAH), West Africa (WAF), Central Africa (CAF), Northeast Africa (NEAF), Southeast Africa (SEAF), West Southern Africa (WSAF), East Southern Africa (ESAF), and Madagascar (MDG). These regions represent distinct climate zones governed by different dynamical regimes, ranging from the hyper-arid Sahara through the monsoon-influenced West African coast, the humid equatorial Congo Basin, the bimodal rainfall regions of East Africa, to the subtropical climates of southern Africa and the island ecosystem of Madagascar. Continental-mean values (AFR) are computed as area-weighted averages across all African land grid cells. This standardized regional framework facilitates direct comparison with IPCC assessments and ensures policy relevance of findings for national adaptation planning (Gutiérrez et al., 2021).

2.2 Observational and Model Datasets

Historical climate observations are derived from the Climatic Research Unit Time-Series version 4.08 (CRU TS4.08) dataset, which provides monthly gridded temperature and precipitation at 0.5° spatial resolution for the period 1901–2023 (Harris et al., 2020). CRU TS4.08 is constructed by interpolating station observations and represents the most comprehensive long-term observational record available for Africa, incorporating over 10,000 stations globally and using quality-controlled homogenization procedures. While station density limitations exist in certain African regions—particularly the Sahara, Congo Basin, and parts of East Africa—CRU remains the standard reference dataset for continental-scale climate trend assessment and model evaluation. The CMIP5 (Table S1) multi-model ensemble mean is constructed from simulations following the experimental protocol of Taylor et al. (2012). Historical simulations span 1850–2005, with future projections extending to 2100 under four Representative Concentration Pathways representing a range of radiative forcing trajectories: RCP2.6 represents strong mitigation with peak forcing around 3.0 W m^{-2} before 2100 and subsequent decline; RCP4.5 represents intermediate stabilization at approximately 4.5 W m^{-2} by 2100; RCP6.0 represents higher stabilization reaching approximately 6.0 W m^{-2} by 2100; and RCP8.5 represents continued high emissions reaching approximately 8.5 W m^{-2} by 2100 (van Vuuren et al., 2011). Monthly near-surface air

https://doi.org/10.5194/egusphere-2026-721
Preprint. Discussion started: 10 March 2026
© Author(s) 2026. CC BY 4.0 License.

temperature and precipitation fields are obtained from the Earth System Grid Federation data portal.

The CMIP6 (Table S2) multi-model ensemble mean follows the experimental design of Eyring et al. (2016), incorporating advances in model physics, higher spatial resolution, and improved representation of Earth system processes, including interactive carbon cycles and atmospheric chemistry. Historical simulations cover 1850–2014, with future projections under four Shared Socioeconomic Pathways that combine radiative forcing levels with socioeconomic narratives: SSP1-2.6 represents a sustainability pathway reaching approximately 2.6 W m^{-2} by 2100; SSP2-4.5 represents a middle-of-the-road development trajectory stabilizing at approximately 4.5 W m^{-2} by 2100; SSP3-7.0 represents regional rivalry with limited climate policy reaching approximately 7.0 W m^{-2} by 2100; and SSP5-8.5 represents fossil-fuelled development reaching approximately 8.5 W m^{-2} by 2100 (O'Neill et al., 2016; Riahi et al., 2017).

To ensure temporal overlap with observational records for model evaluation during the historical analysis period (1980–2020), RCP4.5 and SSP2-4.5 scenarios are used to extend CMIP5 and CMIP6 model simulations through 2006–2020 and 2015–2020, respectively, as these scenarios represent intermediate forcing pathways most consistent with observed emissions during this transition period. All datasets are regridded to a common 1° × 1° spatial resolution using bilinear interpolation for temperature and conservative remapping for precipitation to preserve mass balance. Longitude coordinates are standardized to the range -180° to 180°, and data are subset to the African domain, extending from 35°S to 38°N latitude and 20°W to 52°E longitude. Temperature data originally provided in Kelvin are converted to degrees Celsius, and precipitation flux, expressed as kg m^{-2} s^{-1}, is converted to millimetres per month using appropriate unit conversion factors. Land masks derived from Natural Earth version 5.0.0 at a 1:110 million scale are applied via the regionmask package to exclude oceanic grid cells from all analyses.

2.3 Trend Analysis

Linear trends in temperature and precipitation are computed at each grid cell for the historical period 1980–2020 using ordinary least squares regression on annual mean values. Annual means are computed from monthly data before trend fitting to reduce autocorrelation and provide a robust central estimate of interannual variability. The trend magnitude is expressed as change per decade, with units of °C $decade^{-1}$ for temperature and mm $decade^{-1}$ for precipitation to facilitate interpretation of decadal-scale climate evolution. Statistical significance is assessed using a two-

https://doi.org/10.5194/egusphere-2026-721
Preprint. Discussion started: 10 March 2026
© Author(s) 2026. CC BY 4.0 License.

tailed t-test at the 95% confidence level, with trends considered significant where $p < 0.05$. This approach follows standard practice in climate trend detection studies and provides conservative estimates of forced climate signals emerging from natural variability (IPCC, 2021). Area-weighted regional mean time series are constructed for each IPCC reference region by applying cosine-latitude weighting to account for the decreasing grid cell area toward the poles. The weighting factor for each grid cell is computed as the cosine of latitude in radians, ensuring that tropical grid cells contribute proportionally more to regional averages than high-latitude cells of equivalent angular extent. Regional trends are then computed via linear regression on these area-weighted annual mean time series, with significance testing following the same protocol as spatial trends. This approach provides robust regional-scale trend estimates that account for the uneven spatial distribution of grid cells within irregularly shaped reference regions. Seasonal trends are computed separately for December–January–February (DJF), March–April–May (MAM), June–July–August (JJA), and September–October–November (SON) by extracting corresponding months prior to annual aggregation and trend fitting. This seasonal decomposition reveals the temporal structure of climate trends that may be masked in annual averages, particularly for precipitation, where opposing seasonal signals can cancel when aggregated. Seasonal analysis is essential for African climate assessment, given the strong monsoon influence on rainfall timing across much of the continent.

2.4 Projected Climate Change Analysis

Three 31-year reference periods are defined for climate change assessment to ensure consistency and climatological representativeness: the historical baseline (1975–2005), the near-future period (2035–2065), and the late-century period (2070–2100). The 31-year window length balances the need for climatological representativeness—capturing multiple cycles of interannual variability modes such as the El Niño-Southern Oscillation—with signal detection requirements that favour shorter windows where forced trends are more readily distinguished from internal variability (WMO, 2017). The historical baseline period is centred on the late twentieth century to provide reference conditions prior to the most rapid recent warming, while maintaining sufficient overlap with observational networks for validation. Regional changes are computed from area-weighted spatial means following the cosine-latitude weighting procedure described above, providing robust regional-scale projections that account for spatial heterogeneity within each reference region.

https://doi.org/10.5194/egusphere-2026-721
Preprint. Discussion started: 10 March 2026
© Author(s) 2026. CC BY 4.0 License.

2.5 Compound Hot-Dry Extreme Analysis

Compound hot-dry extremes represent the simultaneous occurrence of anomalously high temperatures and anomalously low precipitation, a combination that generates impacts substantially exceeding those of either stressor acting in isolation through positive feedback mechanisms linking surface energy balance, evapotranspiration, and soil moisture dynamics (Zscheischler et al., 2018; Miralles et al., 2019). Following established methodology in the compound extremes literature (Zscheischler and Seneviratne, 2017; Manning et al., 2019; Bevacqua et al., 2022), compound hot-dry events are defined as months simultaneously satisfying two conditions: temperature exceeding the 90th percentile of the baseline distribution (hot condition) and precipitation falling below the 10th percentile of the baseline distribution (dry condition). These threshold choices identify conditions that are simultaneously anomalously hot and anomalously dry—events occurring with approximately 1% probability under independence assumptions but substantially more frequently due to the negative correlation between temperature and precipitation over land surfaces (Trenberth and Shea, 2005).

Formally, a compound hot-dry event occurs in the month m of year y when:

$$1_{HD}(y,m) = \begin{cases} 1 & \text{if } T(y,m) > T_{90,m} \text{ AND } P(y,m) < P_{10,m} \\ 0 & \text{otherwise} \end{cases} \quad (1)$$

where $T(y,m)$ and $P(y,m)$ are the temperature and precipitation for the year y and month m, $T_{90,m}$ is the 90th percentile of temperature for the calendar month m computed over the baseline period, and $P_{10,m}$ is the 10th percentile of precipitation for the calendar month m. These threshold choices identify conditions that are simultaneously anomalously hot and anomalously dry events occurring with approximately 1% probability under independence assumptions but substantially more frequently due to the negative correlation between temperature and precipitation over land surfaces. Percentile thresholds are computed separately for each calendar month using a month-stratified approach that accounts for seasonal climatology. This stratification prevents artificial inflation of compound frequencies during climatologically dry seasons, where precipitation regularly falls below annual percentile thresholds regardless of whether conditions are anomalous for that time of year. For the calendar month m, the 90th percentile temperature threshold is computed as:

$$T_{90,m} = F_T^{-1}(0.90|\{T(y,m): y \in \text{baseline}\}) \quad (2)$$

where F_T^{-1} denotes the inverse cumulative distribution function (quantile function) of temperature for the month m over the baseline period. The 10th percentile precipitation

https://doi.org/10.5194/egusphere-2026-721
Preprint. Discussion started: 10 March 2026
© Author(s) 2026. CC BY 4.0 License.

threshold $P_{10,m}$ is computed analogously. The baseline period for threshold computation spans 1975–2005. Compound event frequency is computed as the average number of months per year in which both hot and dry conditions are simultaneously satisfied:

$$f_{HD} = \frac{1}{N_{\text{years}}} \sum_{y=1}^{N_{\text{years}}} \sum_{m=1}^{12} 1_{HD}\,(y,m) \tag{3}$$

where N_{years} is the number of years in the analysis period. This metric provides a direct measure of how often populations and ecosystems will experience the combined stress of concurrent heat and moisture deficit. For seasonal analyses, the summation over months is restricted to the three months comprising each season:

$$f_{HD,s} = \frac{1}{N_{\text{years}}} \sum_{y=1}^{N_{\text{years}}} \sum_{m \in s} 1_{HD}\,(y,m) \tag{4}$$

Compound event magnitude integrates both the intensity and frequency of events by computing the cumulative standardized anomaly during compound months. For each compound month, the magnitude contribution is:

$$M(y,m) = 1_{HD}(y,m) \times \left(\frac{T(y,m) - \bar{T}_m}{\sigma_{T,m}} + \frac{\bar{P}_m - P(y,m)}{\sigma_{P,m}} \right) \tag{5}$$

where $\bar{T}_m$ and $\bar{P}_m$ are the baseline climatological means for the month m, and $\sigma_{T,m}$ and $\sigma_{P,m}$ are the corresponding standard deviations. The precipitation term is inverted (baseline minus observed), so drier conditions increase the magnitude. The total magnitude over the analysis period is:

$$M_{\text{total}} = \sum_{y=1}^{N_{\text{years}}} \sum_{m=1}^{12} M\,(y,m) \tag{6}$$

This metric, expressed in units of standard deviations (σ) captures not only how often compound events occur but also how severe they are when they do occur—a distinction critical for impact assessment given the nonlinear relationship between climate stress and system response. Mean event duration is computed as the average length of consecutive compound months. A compound event e is defined as a sequence of one or more consecutive months satisfying the compound criteria. If L_e denotes the length (in months) of the event e and N_{events} is the total number of discrete compound events during the analysis period, mean duration is:

https://doi.org/10.5194/egusphere-2026-721
Preprint. Discussion started: 10 March 2026
© Author(s) 2026. CC BY 4.0 License.

$$D = \frac{\sum_{e=1}^{N_{\text{events}}} L_e}{N_{\text{events}}} \quad (7)$$

This metric distinguishes between climates characterized by frequent but short-lived compound episodes versus those experiencing less frequent but more prolonged compound stress—a distinction with profound implications for ecosystem resilience, agricultural coping capacity, and water reservoir management, where cumulative deficits matter more than instantaneous conditions. Compound event characteristics are computed for two future periods: the mid-century (2035–2065) and the end-century (2070–2100). Both periods are analysed under all available emission scenarios—RCP2.6, RCP4.5, RCP6.0, and RCP8.5 for CMIP5; SSP1-2.6, SSP2-4.5, SSP3-7.0, and SSP5-8.5 for CMIP6—to quantify the scenario dependence of compound risk and identify the mitigation benefit for reducing compound hazard exposure. This comprehensive scenario coverage spans the full range of plausible emission trajectories from aggressive mitigation consistent with Paris Agreement targets to continued fossil fuel dependence, providing decision-relevant information for both adaptation planning under committed warming and mitigation advocacy based on avoided impacts.

3. Result and Discussion

3.1 Recent Trends in Precipitation and Temperature over Africa

Africa has experienced warming over the past four decades, with temperature increases evident across virtually the entire continent (Fig. 1a–c). The observational record reveals continental-mean warming of 0.21°C decade^{-1}, translating to approximately 0.84°C of total warming over the analysis period—a rate that exceeds the global land average (IPCC, 2021). The warming signal is statistically significant across all nine IPCC reference regions, demonstrating that the anthropogenic fingerprint has clearly emerged from natural climate variability across the continent. The spatial structure of observed warming shows distinct geographical patterns that reflect underlying physical mechanisms. The Sahara emerges as the most rapidly warming region (0.23°C decade^{-1}), driven by strong land-atmosphere feedbacks in arid environments where limited soil moisture restricts latent heat flux and amplifies sensible heating (Collins, 2011). Subtropical southern Africa shows comparatively modest warming (0.11–0.13°C decade^{-1}), potentially modulated by oceanic influences. Madagascar shows anomalously strong warming (0.23°C decade^{-1}) relative to mainland regions at similar latitudes, suggesting island-specific responses involving changes in surrounding sea-surface temperatures (Liebmann et al., 2012). Both CMIP5 and CMIP6 ensembles reproduce the broad spatial pattern of continental warming

https://doi.org/10.5194/egusphere-2026-721
Preprint. Discussion started: 10 March 2026
© Author(s) 2026. CC BY 4.0 License.

with notable fidelity, capturing the north-south gradient and the enhanced warming over the Sahara. The Sahara exhibits the strongest simulated warming in both ensembles, with CMIP6 projecting marginally higher trends (0.36°C decade^{-1}) than CMIP5 (0.33°C decade^{-1}), potentially attributable to higher equilibrium climate sensitivity in several CMIP6 models (Meehl et al., 2020).

Precipitation trends reveal a more spatially heterogeneous pattern reflecting the diverse dynamical regimes governing African rainfall (Fig. 1d–f). The observational record indicates significant wetting across much of tropical Africa, with West Africa experiencing the strongest positive trends (3.24 mm decade^{-1}). This wetting pattern is consistent with the well-documented Sahel recovery following the devastating droughts of the 1970s and 1980s (Nicholson, 2013), representing one of the most drastic multidecadal shifts in precipitation observed anywhere on Earth. Central and northeastern Africa show significant moistening (1.23–2.07 mm decade^{-1}), while southeastern Africa exhibits a comparable positive trend (1.94 mm decade^{-1}). Both CMIP ensembles simulate wetting trends over tropical Africa that are directionally consistent with observations, though with varying magnitudes. CMIP6 captures stronger moistening signals than CMIP5 in most regions, with West African trends of 1.75 mm decade^{-1} compared to 0.94 mm decade^{-1} in CMIP5. This improvement may reflect enhanced resolution enabling better representation of mesoscale convective systems. Southern African regions present a contrasting picture, with both model ensembles indicating significant drying trends in eastern southern Africa (−0.54 to −0.76 mm decade^{-1}) and southwestern Africa (−0.32 to −0.34 mm decade^{-1}), aligning with theoretical expectations of poleward expansion of subtropical dry zones under greenhouse warming (Munday and Washington, 2018). Madagascar exhibits the strongest negative precipitation trend among all African regions (−2.11 mm decade^{-1}), in observations. Both model ensembles capture this drying tendency, but with substantially smaller magnitudes (−0.44 to −0.89 mm decade^{-1}), likely driven by changes in Indian Ocean circulation and tropical cyclone behaviour.

Seasonal decomposition reveals important temporal structure in these trends (Figs. S1–S4). Temperature warming is most pronounced during boreal summer (JJA) in the Sahara (0.35–0.38°C decade^{-1} in models) and during austral spring (SON) in eastern southern Africa (0.27–0.28°C decade^{-1}), reflecting season-specific amplification of the warming signal. Precipitation trends show even stronger seasonality: West African wetting peaks during JJA (4.63 mm decade^{-1} observed) coinciding with the monsoon season, while SON exhibits the strongest trends (7.60 mm decade^{-1} observed), suggesting intensification of the late monsoon and its retreat phase. The

https://doi.org/10.5194/egusphere-2026-721
Preprint. Discussion started: 10 March 2026
© Author(s) 2026. CC BY 4.0 License.

DJF season shows pronounced wetting in southeastern Africa (3.99 mm decade^{-1} observed) during the austral summer rainfall season, alongside substantial drying in Madagascar (−6.59 mm decade^{-1}), which dominates the annual signal. These seasonal patterns carry important implications for regional adaptation. The JJA intensification of Sahel rainfall directly benefits rain-fed agriculture that supports hundreds of millions of livelihoods (Sultan and Gaetani, 2016), while the DJF wetting in southeastern Africa enhances water availability during the critical growing season. However, the seasonal concentration of Madagascar's drying during DJF—the primary cyclone and rainfall season—suggests potential disruption of the island's hydrological regime with consequences for rice cultivation and ecosystem function. The regional synthesis (Fig. 1g,h) illuminates continental-scale patterns with greater clarity. Temperature trends are uniformly positive across all regions and datasets, with significance achieved in every case, underscoring the thermodynamically dominated nature of the temperature response to greenhouse forcing. Precipitation trends show pronounced regional dependence in both sign and magnitude, reflecting the greater sensitivity of hydroclimate to circulation changes and internal variability (Rowell et al., 2015). These historical trends establish the baseline against which future climate trajectories must be evaluated, indicating that adaptation measures addressing temperature-related impacts are urgently needed throughout the continent, while water resource planning must account for big regional differences.

https://doi.org/10.5194/egusphere-2026-721
Preprint. Discussion started: 10 March 2026
© Author(s) 2026. CC BY 4.0 License.

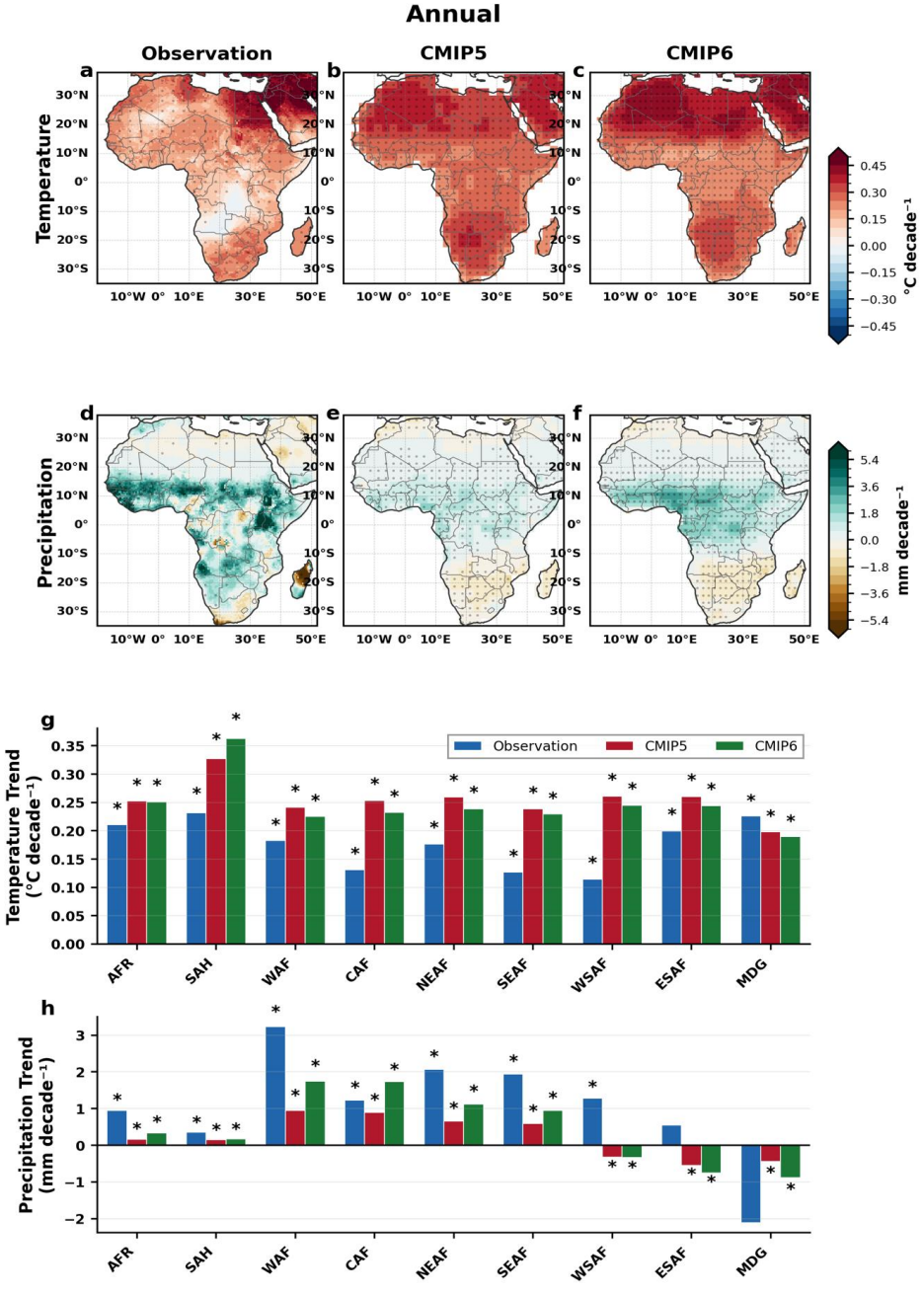

Figure 1: Historical temperature and precipitation trends (1980–2020) across Africa from observations and CMIP model ensembles. (a–c) Spatial distribution of temperature trends (°C decade⁻¹) from CRU TS4.08 observations, CMIP5 multi-model mean, and CMIP6 multi-model mean, respectively. (d–f) Corresponding precipitation trends (mm decade⁻¹). Stippling indicates statistical significance ($p < 0.05$). (g,h) Regional mean trends for temperature and precipitation

https://doi.org/10.5194/egusphere-2026-721
Preprint. Discussion started: 10 March 2026
© Author(s) 2026. CC BY 4.0 License.

across IPCC AR6 African reference regions, with asterisks denoting significant trends. Note: RCP4.5 and SSP2-4.5 scenarios are used to extend model simulations from 2006–2020 and 2015–2020, respectively, to ensure temporal overlap with the observational period

3.2 Projected Regional Climate Changes

Projected temperature changes across African regions exhibit a clear emission-dependent trajectory (Fig. 2). By mid-century (2035–2065), all regions experience warming of 0.9–2.5°C, depending on the scenario, with the Sahara consistently the most rapidly warming region. Under low-emission pathways (RCP2.6/SSP1-2.6), mid-century warming remains below 1.5°C across most regions, while high-emission scenarios (RCP8.5/SSP5-8.5) drive Saharan warming exceeding 2°C. Late-century projections reveal drastic amplification scaling with cumulative emissions. Under continued high emissions, African temperatures increase by 3.0–5.3°C above the historical baseline, with the Sahara experiencing extreme warming of 4.6°C (CMIP5) to 5.3°C (CMIP6). Such magnitudes would fundamentally transform African climate regimes (Engelbrecht et al., 2015). Continental-mean warming reaches 3.7°C under RCP8.5 and 4.2°C under SSP5-8.5, substantially exceeding Paris Agreement targets (UNFCCC, 2015). Under aggressive mitigation (RCP2.6/SSP1-2.6), late-century warming stabilizes at 0.9–1.8°C. CMIP6 projections consistently exceed CMIP5 values by 0.3–0.7°C, reflecting higher equilibrium climate sensitivity in many CMIP6 models (Zelinka et al., 2020). Madagascar experiences the most modest warming (1.6–3.5°C by the late century), moderated by oceanic thermal inertia. Precipitation projections reveal regional wetting and drying tendencies that intensify with radiative forcing. The Sahara, Sahel, and tropical African regions exhibit consistent positive precipitation changes, with late-century increases reaching 5–15% under CMIP5 and 10–35% under CMIP6 high-emission scenarios. This projected wetting aligns with theoretical expectations of northward migration of tropical rain belts (Chou et al., 2009). Southeast Africa presents the strongest wetting signal, with CMIP6 projecting increases exceeding 30% under SSP5-8.5. In contrast, southern African regions (WSAF, ESAF) and Madagascar exhibit consistent drying of 2–10%, representing serious water security concerns. These tendencies align with the projected poleward expansion of subtropical dry zones (Munday and Washington, 2018).

Seasonal decomposition reveals important temporal structure in projected changes (Figs. S5–S8). Temperature projections show maximum Saharan warming during JJA (4.9°C under RCP8.5; 5.7°C under SSP5-8.5), reflecting amplified summer heating in arid environments. Southern African regions exhibit the strongest warming during SON (4.0–4.6°C under high emissions),

https://doi.org/10.5194/egusphere-2026-721
Preprint. Discussion started: 10 March 2026
© Author(s) 2026. CC BY 4.0 License.

coinciding with the pre-summer heating season. Precipitation seasonality shows pronounced regional dependence. West African JJA precipitation increases by 5–8% (CMIP5) and 8–15% (CMIP6) under high emissions, with implications for monsoon-dependent agriculture. The Saharan wetting signal peaks during JJA and SON, suggesting northward expansion of the summer monsoon. Southern African drying is most pronounced during MAM and SON (5–12% decreases), threatening the shoulder seasons critical for agricultural planning. Madagascar experiences year-round drying, with the strongest during DJF (−5 to −12%), the primary rainfall season, with severe implications for rice cultivation and water resources. These projections underscore the urgency of both mitigation and adaptation. The substantial spread of scenarios demonstrates that emission choices will determine whether African warming remains manageable (1–2°C) or reaches transformative levels (4–5°C), while the spatial heterogeneity of precipitation responses necessitates regionally tailored adaptation strategies (Trisos et al., 2022).

https://doi.org/10.5194/egusphere-2026-721
Preprint. Discussion started: 10 March 2026
© Author(s) 2026. CC BY 4.0 License.

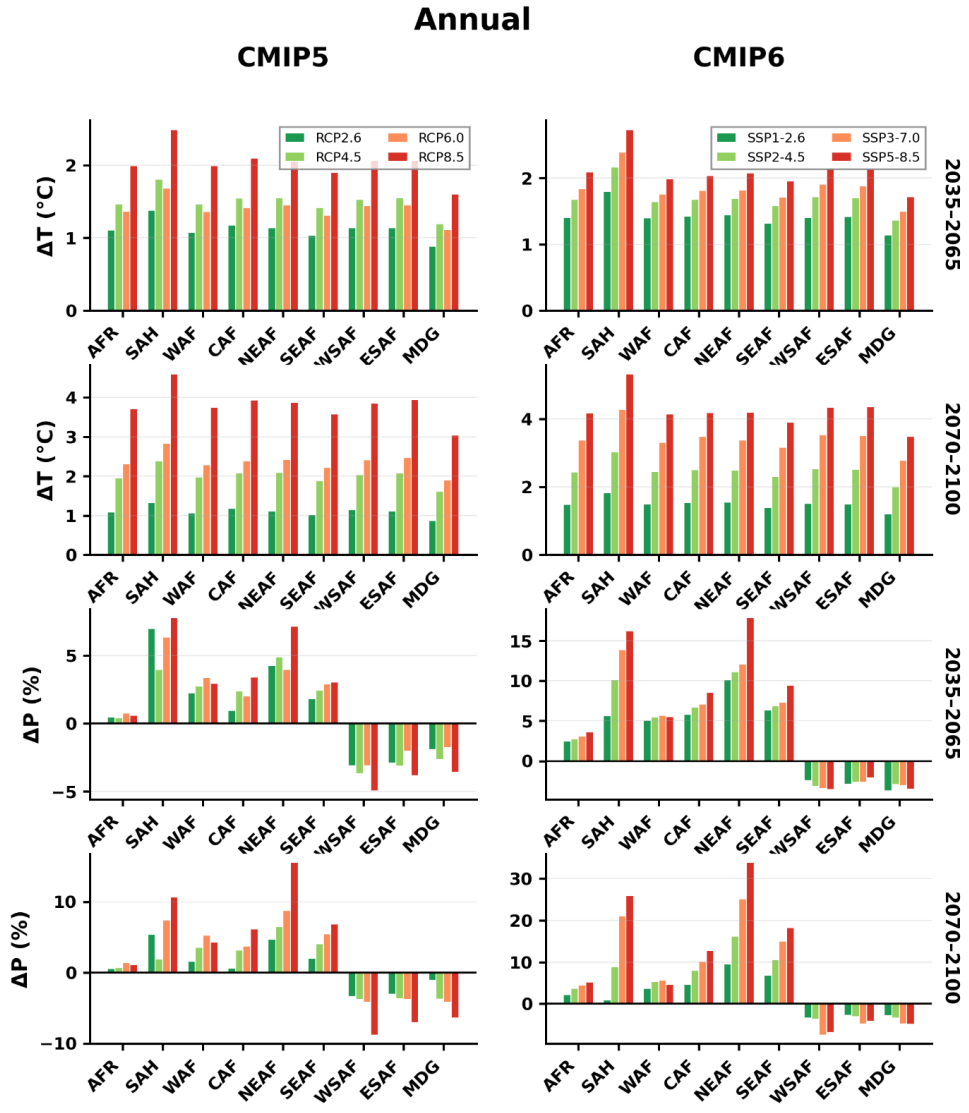

Figure 2: **Projected regional mean temperature and precipitation changes across African IPCC reference regions under CMIP5 and CMIP6 emission scenarios.** Left panels show CMIP5 projections (RCP2.6, RCP4.5, RCP6.0, RCP8.5); right panels show CMIP6 projections (SSP1-2.6, SSP2-4.5, SSP3-7.0, SSP5-8.5). Rows display: near-future (2035–2065) temperature change (°C), late-century (2070–2100) temperature change (°C), near-future precipitation change (%), and late-century precipitation change (%), all relative to the 1975–2005 baseline.

3.3 Projected Change in Compound Hot-Dry Extremes

Compound hot-dry extremes—defined as the simultaneous occurrence of anomalously high temperatures (>90th percentile) and low precipitation (<10th percentile)—represent a

https://doi.org/10.5194/egusphere-2026-721
Preprint. Discussion started: 10 March 2026
© Author(s) 2026. CC BY 4.0 License.

particularly severe climate hazard with disproportionate impacts on agriculture, water resources, and human health compared to either stressor acting alone (Zscheischler et al., 2018). Both CMIP5 and CMIP6 ensembles project substantial increases in compound event frequency across Africa, with pronounced spatial heterogeneity and strong temporal amplification from mid to the end of the century (Figs 3 and 4). Southern Africa emerges as the continental hotspot for compound extremes across both time horizons. By mid-century (2035–2065), western southern Africa (WSAF) experiences compound frequencies of 0.26–0.41 months per year (CMIP5) and 0.33–0.43 months per year (CMIP6), with eastern southern Africa (ESAF) showing comparable values (Fig. 3i,j). This regional vulnerability intensifies markedly by the end of the century (2070–2100), with WSAF frequencies reaching 0.25–0.58 months per year under CMIP5 and 0.36–0.62 months per year under CMIP6 high-emission scenarios (Fig. 4i,j). The doubling of compound frequency between time periods under high emissions underscores the accelerating nature of compound risk. The Sahara exhibits substantial compound frequencies despite projected increases in precipitation, reaching 0.21–0.31 months per year by mid-century and 0.25–0.44 months per year by end-century under high emissions.

This counterintuitive result indicates that the magnitude of Saharan warming is sufficient to drive compound events even where mean rainfall is increasing, emphasizing that temperature extremes can dominate compound risk independent of precipitation trends (Vogel et al., 2019). Tropical African regions (WAF, CAF, NEAF, SEAF) show consistently lower compound frequencies, reflecting the combination of more modest warming with projected wetting. Northeast Africa exhibits the lowest compound risk across both ensembles and time periods (0.02–0.05 months per year), consistent with its substantial projected increases in precipitation that counteract warming. However, even these relatively protected regions show increased compound frequency by end-century, with West Africa rising from 0.08–0.15 months per year at mid-century to 0.11–0.22 months per year by 2070–2100 under high emissions. The scenario dependence of compound frequency strengthens markedly between time periods. At mid-century, continental-mean compound frequency increases by approximately 30–50% across low- and high-emission pathways. By end-century, this spread widens substantially: continental-mean frequencies reach 1.9–2.2 months per year under low emissions versus 3.2–3.7 months per year under high emissions—a near-doubling that emphasizes the substantial mitigation benefit for reducing compound risk. WSAF shows the largest absolute scenario spread, with end-century frequencies of 0.25 months per year (RCP2.6) versus 0.58 months per year (RCP8.5) in CMIP5, representing a 130% increase under high emissions. CMIP5 and CMIP6 show broadly consistent spatial patterns, with both ensembles identifying southern Africa as the primary vulnerability hotspot.

https://doi.org/10.5194/egusphere-2026-721
Preprint. Discussion started: 10 March 2026
© Author(s) 2026. CC BY 4.0 License.

However, notable differences emerge. CMIP6 projects higher compound frequencies in tropical regions under equivalent forcing levels, potentially reflecting enhanced hydrological sensitivity. Conversely, CMIP5 projects slightly higher peak frequencies in WSAF under RCP8.5 (0.58 months per year) than CMIP6 under SSP5-8.5 (0.62 months per year), though the difference is modest.

Seasonal decomposition reveals strong and regionally differentiated temporal structure in compound hot–dry risk across Africa (Figs. S9–S16). During DJF, compound-event frequencies are highest over northern Africa and the Sahara, reaching approximately 0.10–0.16 months per season by the end of the century under high-emission scenarios, representing roughly a 50–80% increase relative to mid-century levels. In MAM, elevated compound frequencies extend across the Sahel and southern Africa, with end-century values commonly exceeding 0.08–0.14 months per season, indicating heightened exposure during key agricultural transition and planting periods. During JJA, compound hot–dry risk exhibits a pronounced signal over southern Africa, with event frequencies increasing from ~0.06-0.12 months per season in the near term to approximately 0.08–0.18 months per season by the end of the century, while remaining comparatively limited across monsoon-dominated West Africa. In contrast, northern Africa shows localized compound risk associated with persistent aridity, but without the widespread intensification observed over southern Africa during this season. The SON season exhibits the most pronounced amplification in southern Africa, where compound-event frequencies increase from approximately 0.06–0.12 months per season in the near term to >0.12 months per season by the end of the century, effectively doubling in several subregions. Across all seasons, compound hot–dry frequencies show a consistent upward trajectory from mid-century to end-century under high-emission pathways, with the strongest absolute and relative increases occurring in regions already experiencing chronic water stress. These projected changes have serious implications for African food security, as compound extremes are known to cause disproportionately large crop-yield losses compared with single-driver events (Lesk et al., 2016). The substantial inter-scenario spread is evident in Figs. S9–S16 indicate that mitigation can reduce late-century compound frequencies by 30–50% in several regions, underscoring a clear and quantifiable co-benefit of emission reductions: limiting compound climate hazards and enhancing long-term climate resilience across Africa (Zscheischler and Seneviratne, 2017).

https://doi.org/10.5194/egusphere-2026-721
Preprint. Discussion started: 10 March 2026
© Author(s) 2026. CC BY 4.0 License.

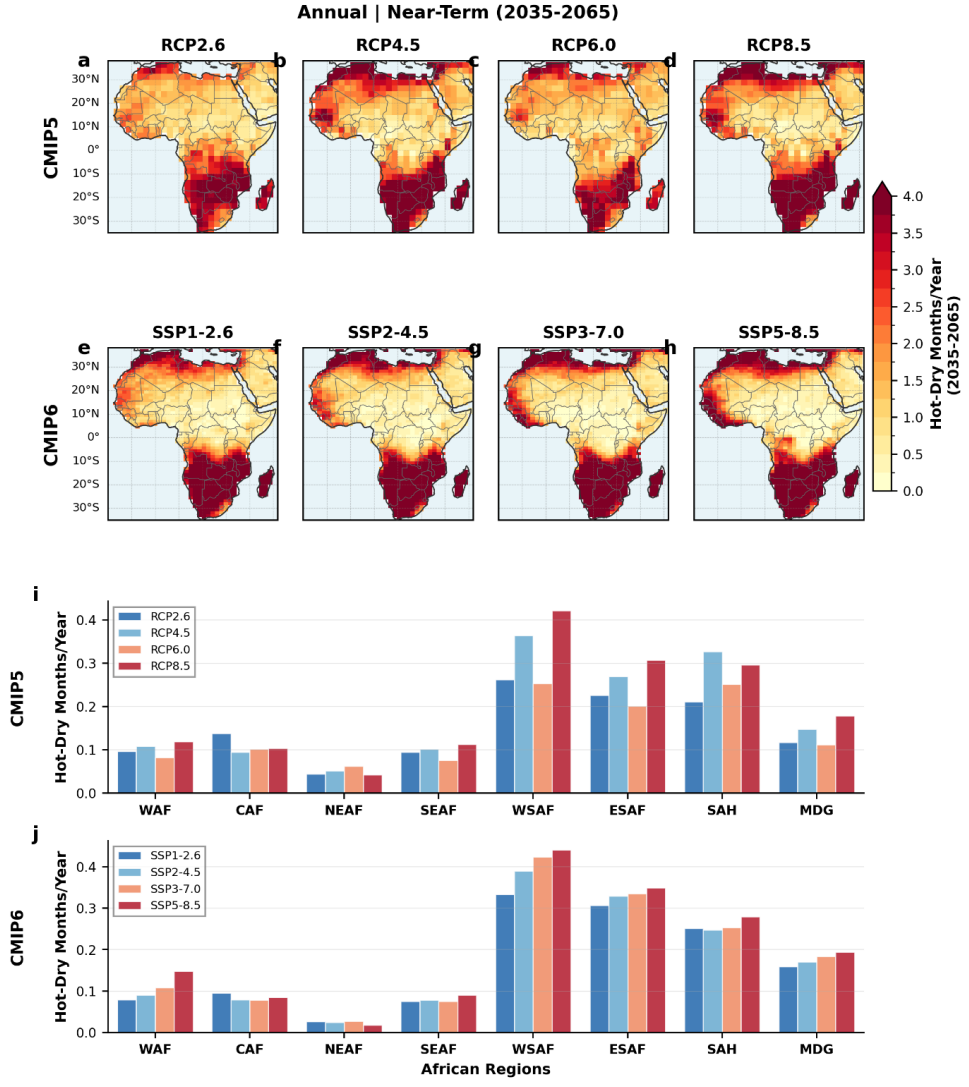

Figure 3: Projected frequency of compound hot-dry extremes across Africa for the near-term period (2035–2065). (a–d) Spatial distribution of annual hot-dry months per year from CMIP5 under RCP2.6, RCP4.5, RCP6.0, and RCP8.5 scenarios, respectively. (e–h) Corresponding projections from CMIP6 under SSP1-2.6, SSP2-4.5, SSP3-7.0, and SSP5-8.5 scenarios. (i,j) Regional mean compound event frequency (hot-dry months per year) across African IPCC reference regions for CMIP5 and CMIP6.

https://doi.org/10.5194/egusphere-2026-721
Preprint. Discussion started: 10 March 2026
© Author(s) 2026. CC BY 4.0 License.

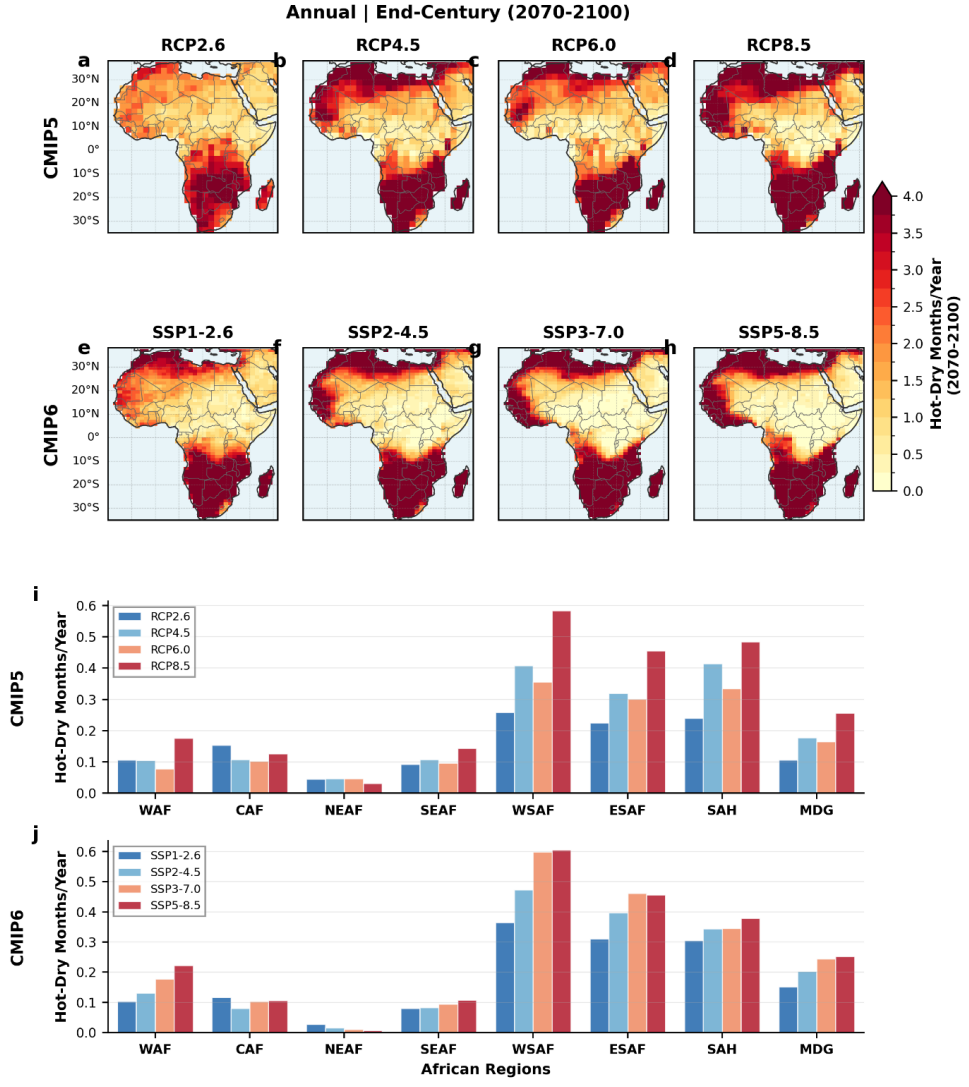

Figure 4: Projected frequency of compound hot-dry extremes across Africa for the end-century period (2070–2100). Layout and definitions as in Fig. 3.

3.4 Compound Event Magnitude and Duration

Beyond frequency, the severity of compound hot-dry extremes depends critically on their magnitude and duration—characteristics that determine cumulative stress on agricultural systems, water resources, and human health (Zscheischler et al., 2020). By the end of the century, both CMIP5 and CMIP6 projects substantial increases in the magnitude and duration of compound events, with southern Africa experiencing the most severe intensification (Figs. 5, 6). Compound event magnitude—expressed as cumulative standardized anomalies integrating both intensity and

https://doi.org/10.5194/egusphere-2026-721
Preprint. Discussion started: 10 March 2026
© Author(s) 2026. CC BY 4.0 License.

frequency—shows drastic spatial heterogeneity and strong scenario dependence (Fig. 5). Southern Africa emerges as the epicentre of severe compound stress, with WSAF and ESAF experiencing cumulative magnitudes of 4–11σ under CMIP5 high emissions and 6–13σ under CMIP6 SSP5-8.5. These values represent extraordinary departures from baseline climate, indicating that end-century compound events will not only be more frequent but also substantially more intense than historical analogues. The nonlinear scaling with radiative forcing is particularly striking: WSAF magnitude increases from approximately 1.5σ under RCP2.6 to 11σ under RCP8.5—a seven-fold amplification that far exceeds the linear scaling of mean temperature change.

Madagascar exhibits unexpectedly high compound magnitude under CMIP6 projections, reaching 6–12σ under SSP3-7.0 and SSP5-8.5 despite moderate increases in frequency. This pattern suggests that when compound events occur over Madagascar, they are particularly intense, likely reflecting the island's vulnerability to simultaneous warming and disruption of Indian Ocean moisture transport. The contrast between relatively modest frequency and high magnitude underscores that frequency alone does not fully characterize compound risk. Tropical regions (WAF, CAF, NEAF) show substantially lower magnitudes (1–8σ, depending on scenario), consistent with the protective effect of projected increases in precipitation. However, even these regions experience meaningful magnitude increases under high emissions, with West Africa reaching 7–8σ under RCP8.5/SSP5-8.5—sufficient to cause significant agricultural and ecological impacts during event years. The Sahara presents an interesting case in which moderate-magnitude (1–4σ) events are relatively frequent, suggesting that Saharan compound events are frequent but individually less intense than those in southern Africa. This pattern reflects the already extreme aridity of the region, which limits the potential for precipitation to fall further below climatological values as temperatures continue to rise. Compound event duration exhibits equally concerning patterns, with mean event length increasing substantially under high emissions (Fig. 6).

Southern African regions show the longest projected durations, with WSAF events averaging 2.3 months under RCP4.5, rising to 4.8 months under RCP8.5 in CMIP5, and 2.0 months under SSP1-2.6, rising to 5.5 months under SSP5-8.5 in CMIP6. These multi-month compound events represent persistent drought-heat stress that would severely challenge agricultural systems and deplete water reserves. ESAF shows comparable patterns, with durations reaching 4.0–5.2 months under high-emission scenarios. The duration results reveal that compound events are not merely becoming more frequent but are transitioning from discrete monthly anomalies to sustained multi-month episodes. Under baseline conditions, compound events typically persist for 1–1.5 months. By the end of the century, under high emissions, southern African events extend

https://doi.org/10.5194/egusphere-2026-721
Preprint. Discussion started: 10 March 2026
© Author(s) 2026. CC BY 4.0 License.

to 4–6 months on average, fundamentally shifting the nature of compound risk from acute shocks to chronic stress. Madagascar again shows elevated duration under CMIP6 (4.5–5.2 months under SSP3-7.0/SSP5-8.5), reinforcing its emergence as a compound risk hotspot in the newer model generation. The combination of high magnitude and extended duration indicates that Malagasy compound events could persist for entire growing seasons, with catastrophic implications for the island's agriculture.

Tropical regions maintain relatively shorter durations (1.0–2.2 months) across scenarios, indicating that while these regions may occasionally experience compound conditions, events remain episodic rather than persistent. NEAF shows the shortest durations (0.8–1.1 months), consistent with its robust projected wetting that rapidly terminates compound conditions. The scenario sensitivity of both magnitude and duration exceeds that of frequency, indicating that the character of compound events changes more markedly than their occurrence rate. Under low emissions, compound events remain moderate in both intensity and persistence, resembling enhanced versions of historical extremes. Under high emissions, compound events transform into qualitatively different phenomena—prolonged, intense stress episodes that exceed historical experience by substantial margins. CMIP6 consistently projects higher magnitudes and longer durations than CMIP5 for equivalent forcing levels, particularly in southern Africa and Madagascar. This difference likely reflects the higher climate sensitivity and stronger land-atmosphere feedbacks in CMIP6 models, which amplify compound event characteristics beyond frequency changes alone (Seneviratne et al., 2021). The combination of increased frequency (Figs. 3, 4), amplified magnitude, and extended duration creates a compound risk trajectory in which southern African populations face not only more events but also qualitatively worse events. Traditional coping mechanisms calibrated to historical drought-heat episodes may prove inadequate for multi-month compound events of unprecedented intensity. The strong scenario dependence demonstrates that mitigation remains a powerful lever for limiting compound risk, with low-emission pathways maintaining event characteristics closer to historical norms, while high-emission pathways drive a transformation toward a fundamentally more hostile climate regime (AghaKouchak et al., 2020).

https://doi.org/10.5194/egusphere-2026-721
Preprint. Discussion started: 10 March 2026
© Author(s) 2026. CC BY 4.0 License.

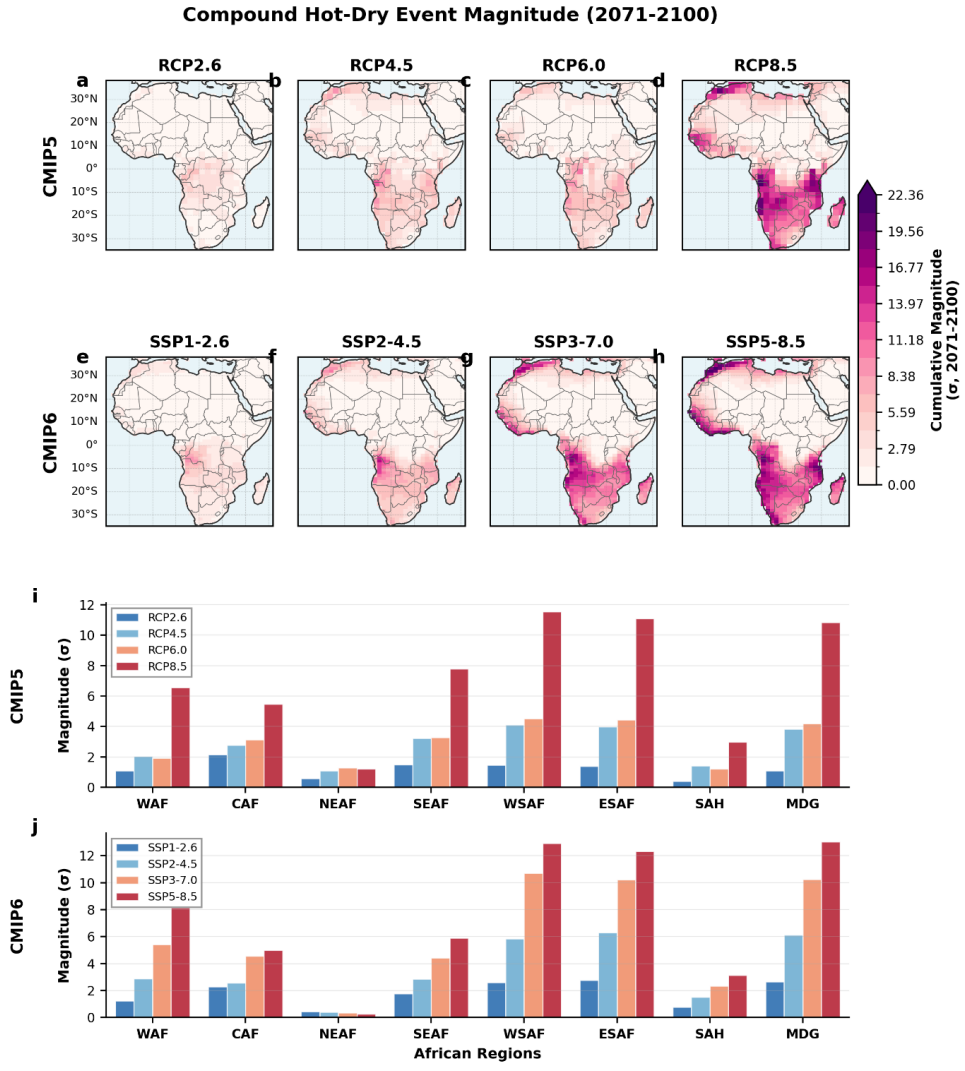

Figure 5: Projected magnitude of compound hot-dry events across Africa for the end-century period (2070–2100). (a–d) Spatial distribution of cumulative compound magnitude (expressed in standard deviations, σ) from CMIP5 under RCP2.6, RCP4.5, RCP6.0, and RCP8.5 scenarios, respectively. (e–h) Corresponding projections from CMIP6 under SSP1-2.6, SSP2-4.5, SSP3-7.0, and SSP5-8.5 scenarios. (i,j) Regional mean compound magnitude across African IPCC reference regions for CMIP5 and CMIP6, respectively. Magnitude is computed as the cumulative standardized anomaly during compound events, integrating both intensity and frequency.

https://doi.org/10.5194/egusphere-2026-721
Preprint. Discussion started: 10 March 2026
© Author(s) 2026. CC BY 4.0 License.

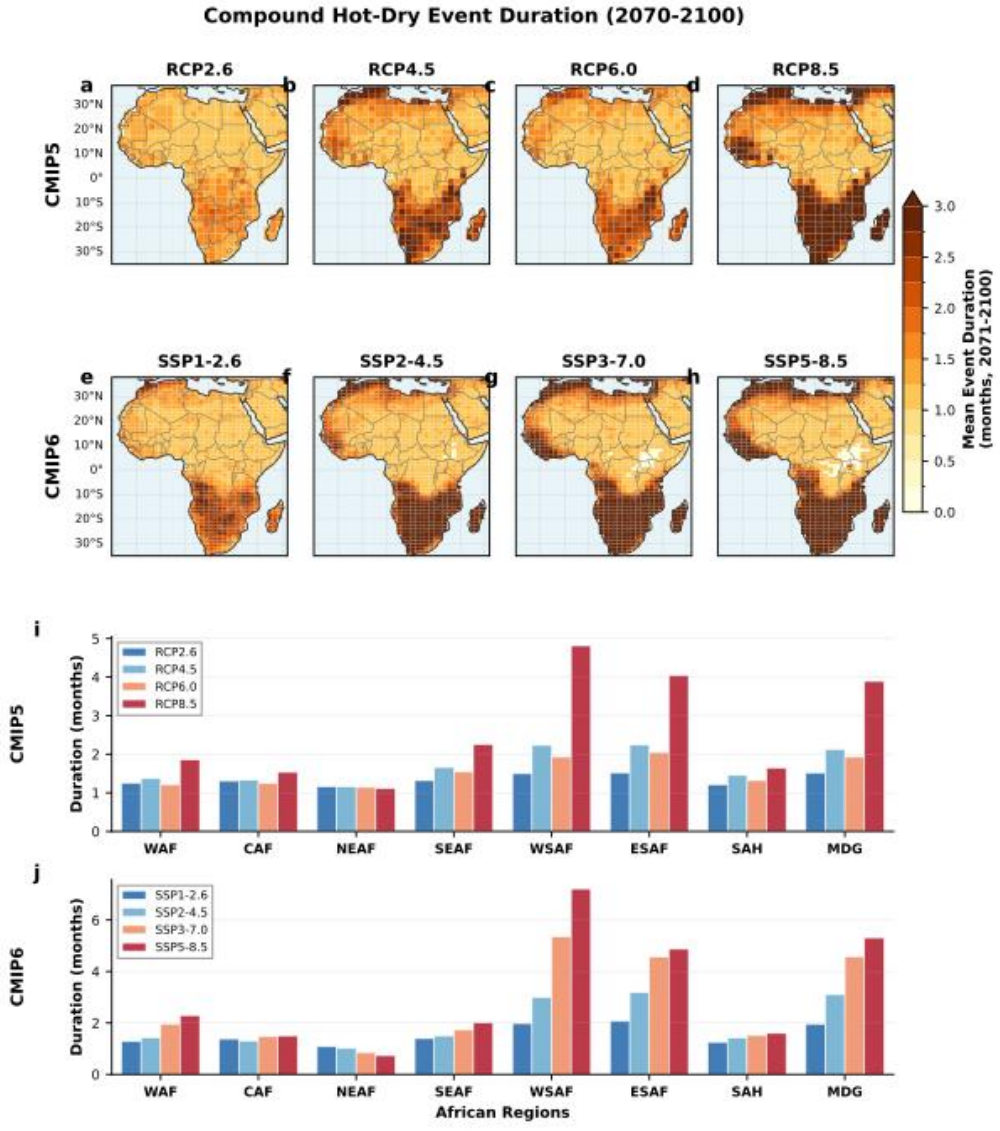

Figure 6: Projected mean duration of compound hot-dry events across Africa for the end-century period (2070–2100). (a–d) Spatial distribution of mean event duration (months) from CMIP5 under RCP2.6, RCP4.5, RCP6.0, and RCP8.5 scenarios, respectively. (e–h) Corresponding projections from CMIP6 under SSP1-2.6, SSP2-4.5, SSP3-7.0, and SSP5-8.5 scenarios. (i,j) Regional mean compound duration across African IPCC reference regions for CMIP5 and CMIP6, respectively. Duration represents the average length of consecutive compound months per event

https://doi.org/10.5194/egusphere-2026-721
Preprint. Discussion started: 10 March 2026
© Author(s) 2026. CC BY 4.0 License.

3.5 Climate Drivers of Compound Hot-Dry Extreme Intensification

The spatial pattern of compound hot–dry extreme intensification across Africa is primarily controlled by regional precipitation changes, which are the dominant modulators of compound vulnerability against a backdrop of near-uniform warming (Fig. 7a–h). Across all emission scenarios and both CMIP generations, a robust inverse relationship emerges between precipitation change and compound hot–dry frequency (r^2 = 0.47–0.71), indicating that regions experiencing drying undergo substantially stronger increases in compound extremes, whereas regions with increasing precipitation exhibit muted responses despite comparable warming. The fitted regression slopes (k = −0.017 to −0.033 months yr^{-1} per mm $month^{-1}$) quantify this sensitivity, implying that each mm per month of regional drying induces approximately 0.02–0.03 additional compound hot–dry months per year. This sensitivity is consistent with earlier regional and global assessments, which show that precipitation deficits account for 50–80% of drought intensity variability by regulating soil moisture availability and land–atmosphere coupling strength (Berg and Sheffield, 2018; Manning et al., 2019).

The clustering of African subregions within precipitation compound response space reveals distinct vulnerability regimes governed by underlying physical mechanisms. Southern African regions (WSAF and ESAF) consistently occupy the high-vulnerability quadrant, characterized by concurrent precipitation decreases (−2 to −4 mm $month^{-1}$) and the largest increases in compound hot–dry frequency (0.25–0.62 months yr^{-1}). This double exposure reflects the reinforcing effects of subtropical drying and thermodynamic warming. Poleward expansion of the Hadley circulation reduces moisture convergence and suppresses rainfall, while rising temperatures enhance atmospheric evaporative demand, accelerating soil moisture depletion (Archer et al., 2021; Maúre et al., 2018). Reduced soil moisture limits latent heat flux and enhances sensible heating, further amplifying surface temperatures and creating a positive feedback loop that intensifies both the heat and dryness components of compound extremes (Miralles et al., 2019; Zhou et al., 2019). These feedbacks explain why southern Africa emerges as the continental epicentre of compound hot–dry risk across all scenarios and time horizons.

In contrast, NEAF consistently occupies a low-vulnerability regime, combining substantial precipitation increases (+2 to +8 mm $month^{-1}$) with minimal changes in compound frequency (0.02–0.05 months yr^{-1}). Enhanced monsoon circulation and a northward shift of tropical rain belts under greenhouse warming increase moisture availability and evaporative cooling, offsetting warming-induced stress and reducing the likelihood that precipitation falls below extreme dry thresholds (Chou et al., 2009; Rowell et al., 2015). This result demonstrates that sufficient increases in precipitation can partially decouple compound hot–dry risk from temperature rise,

https://doi.org/10.5194/egusphere-2026-721
Preprint. Discussion started: 10 March 2026
© Author(s) 2026. CC BY 4.0 License.

even under strong radiative forcing. The contrast between southern and northeastern Africa underscores the need for regionally differentiated adaptation strategies: southern Africa requires integrated responses to simultaneous heat and water scarcity, whereas NEAF may prioritize managing increased rainfall variability and flood risk over compound drought–heat stress.

The Sahara (SAH) represents an intermediate but instructive case. Despite modest projected increases in mean precipitation, compound hot–dry frequency rises substantially (0.21–0.44 months yr^{-1} under high-emission scenarios). This apparent paradox highlights the dominant role of extreme warming in hyper-arid environments, where baseline precipitation is already near the lower bound of climatological variability. In such settings, even small negative deviations relative to the 10th-percentile threshold can coincide with extreme temperatures, resulting in frequent compound conditions regardless of mean wetting trends. This finding reinforces that compound risk cannot be inferred from precipitation projections alone, particularly in arid regions where thermodynamic forcing overwhelms hydrological moderation. MDG exhibits pronounced scenario sensitivity, transitioning from moderate vulnerability under low-emission pathways to high vulnerability under strong warming. Under high-emission scenarios, MDG experiences drying of -3 to -4 mm $month^{-1}$ accompanied by sharp increases in compound frequency, aligning it more closely with southern African response patterns. While Indian Ocean warming and circulation changes have previously been linked to Malagasy drying (Liebmann et al., 2012), this study provides the first systematic demonstration of how these precipitation changes translate into intensified compound hot–dry extremes, posing substantial risks to agriculture and the island's biodiversity.

An intergenerational comparison reveals that CMIP6 models consistently produce stronger precipitation–compound relationships (r^2 = 0.59–0.71) than CMIP5 (r^2 = 0.47–0.61), particularly under higher-emission scenarios. This strengthening likely reflects improved representation of land surface processes, soil moisture dynamics, and land–atmosphere coupling in CMIP6, enabled by enhanced parameterizations and higher spatial resolution (Seneviratne et al., 2021). The systematic increase in explained variance with radiative forcing—from $r^2 \approx 0.59$ under SSP1-2.6 to $r^2 \approx 0.71$ under SSP5-8.5—indicates that precipitation-temperature coupling intensifies nonlinearly as the climate departs further from the historical baseline. This behaviour is consistent with theoretical and observational evidence that land–atmosphere feedbacks strengthen under higher warming levels, amplifying compound extremes beyond linear expectations (Hirschi et al., 2011; Zhou et al., 2019). Importantly, this implies that delayed mitigation not only increases compound risk magnitude but also enhances the physical coupling mechanisms that generate

https://doi.org/10.5194/egusphere-2026-721
Preprint. Discussion started: 10 March 2026
© Author(s) 2026. CC BY 4.0 License.

compound extremes, thereby reducing the effectiveness of adaptation measures calibrated to historical climate behaviour.

While precipitation change governs the spatial differentiation of compound vulnerability, temperature change provides the universal thermodynamic driver underlying compound hot–dry intensification across all African regions (Fig. 8). A positive relationship between regional warming and compound frequency change is evident across scenarios and models, with sensitivities ranging from 0.14 to 0.53 additional compound months per year per degree Celsius of warming. This confirms that greenhouse warming systematically increases compound risk, even in regions experiencing increased precipitation. However, the temperature–compound relationship exhibits substantially lower explanatory power (r^2 = 0.12–0.52) than the precipitation-based relationship, reflecting the relatively uniform spatial distribution of projected African warming (2–5°C across most regions by late century) compared with the strong spatial heterogeneity of precipitation responses. Temperature thus sets the baseline escalation of compound risk, while precipitation anomalies determine where this escalation becomes most severe.

Taken together, these results demonstrate that compound hot–dry extreme intensification across Africa arises from the interaction of a spatially uniform thermodynamic forcing with highly heterogeneous hydrological responses. Regions experiencing concurrent warming and drying—particularly southern Africa and MDG under high-emission scenarios—face a nonlinear escalation of compound risk driven by reinforcing land–atmosphere feedbacks. Conversely, regions with robust precipitation increases can partially offset warming-induced stress, though they do not eliminate the compound risk entirely. The stronger coupling and higher sensitivities projected by CMIP6 suggest that earlier assessments based on CMIP5 may underestimate future compound vulnerability, especially under high-emission pathways. From an adaptation and mitigation perspective, these findings carry clear implications. First, compound risk hotspots cannot be identified from temperature or precipitation projections in isolation; integrated assessments are essential. Second, mitigation yields dual benefits: it limits both the magnitude of warming and the strength of land–atmosphere feedbacks that amplify compound extremes. Finally, adaptation strategies must be region-specific, targeting chronic heat–water stress in southern Africa while addressing shifting precipitation regimes and variability elsewhere. As warming progresses, failure to account for the coupled nature of temperature and moisture extremes risks substantial underestimation of future climate impacts across Africa.

https://doi.org/10.5194/egusphere-2026-721
Preprint. Discussion started: 10 March 2026
© Author(s) 2026. CC BY 4.0 License.

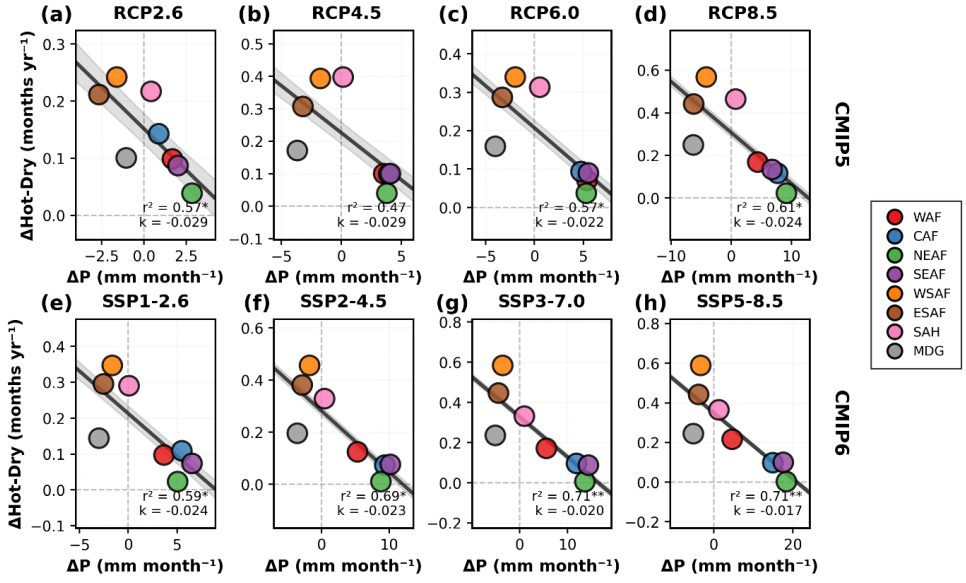

Figure 7. Precipitation control on compound hot-dry extreme intensification across African regions. Scatter plots showing the relationship between precipitation change (ΔP, mm month⁻¹) and change in compound hot-dry month frequency (ΔHot-Dry, months yr⁻¹) for eight African IPCC AR6 reference regions during 2071–2100 relative to 1986–2014 baseline. **(a–d)** CMIP5 projections under RCP2.6, RCP4.5, RCP6.0, and RCP8.5 scenarios, respectively. **(e–h)** Corresponding CMIP6 projections under SSP1-2.6, SSP2-4.5, SSP3-7.0, and SSP5-8.5 scenarios. Black lines show linear regression fits with 95% confidence intervals (gray shading). Statistics boxes display coefficient of determination (r^2), slope (k), and statistical significance (asterisks: * $p < 0.05$, ** $p < 0.01$).

https://doi.org/10.5194/egusphere-2026-721
Preprint. Discussion started: 10 March 2026
© Author(s) 2026. CC BY 4.0 License.

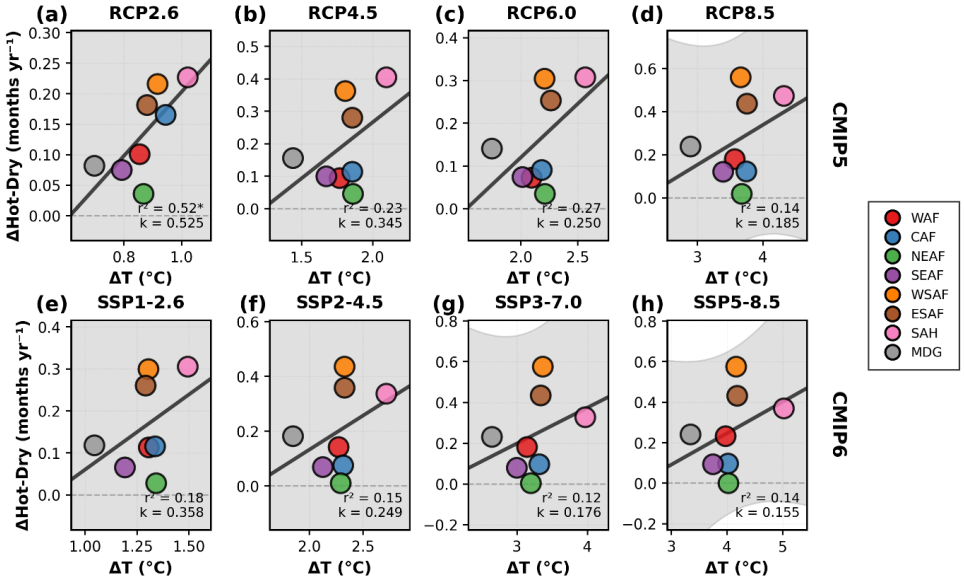

Figure 8: same as Figure 7, but for Temperature.

4. CONCLUSION

This study provides the first continent-wide, multi-generation assessment of compound hot–dry extreme evolution across Africa, demonstrating that concurrent temperature–precipitation extremes will intensify substantially throughout the twenty-first century with far-reaching implications for climate-sensitive systems. By integrating CMIP5 and CMIP6 multi-model ensembles across the full range of emission scenarios, we show that compound climate risk in Africa arises from a hierarchical driver structure: accelerated warming acts as a universal thermodynamic forcing, while regional precipitation trajectories govern the spatial distribution and severity of compound vulnerability. This framework fundamentally distinguishes compound risk from single-variable extremes and has direct implications for adaptation planning and mitigation prioritization across African climate zones.

Observational evidence indicates that Africa has already undergone compound-relevant climate shifts, with continent-wide warming of approximately 0.21 °C decade^{-1} during 1980–2020, accompanied by strongly heterogeneous precipitation trends. Both CMIP5 and CMIP6 ensembles reproduce the large-scale spatial patterns of historical warming and precipitation change with reasonable fidelity, lending confidence to their projections. However, CMIP6 consistently projects stronger future intensification of compound hot–dry extremes than CMIP5, reflecting higher climate sensitivity and enhanced representation of land–atmosphere coupling processes critical for compound event development.

https://doi.org/10.5194/egusphere-2026-721
Preprint. Discussion started: 10 March 2026
© Author(s) 2026. CC BY 4.0 License.

Southern Africa emerges robustly as the continental epicentre of compound hot–dry risk. By the end of the century, western and eastern southern Africa experience compound frequencies of 0.36–0.62 months yr^{-1} under high-emission scenarios—more than double those under strong mitigation pathways. Importantly, compound risk intensification is not limited to frequency alone. Event characteristics undergo a qualitative transformation: cumulative compound event magnitudes exceed 10–13 standard deviations in southern Africa and Madagascar, while mean event duration lengthens from approximately 1–1.5 months historically to 4–6 months under high emissions. This shift from episodic anomalies to prolonged multi-month stress fundamentally alters the nature of climate risk, suggesting that coping strategies calibrated to historical drought or heat events may be insufficient under future conditions.

A key finding of this study is that regional precipitation changes account for 60–70% of the spatial variance in compound hot–dry extreme intensification, whereas temperature changes account for only 10–20% in next-generation models. Although warming is explicitly embedded in the compound-event definition and increases exceedance probabilities everywhere, projected African warming is relatively uniform in space (≈2–5 °C by the late century). In contrast, precipitation responses vary strongly across regions, ranging from robust wetting (+10 to +30%) in northeastern Africa to pronounced drying (−5 to −15%) in southern Africa. This heterogeneity determines whether thermodynamic warming translates into moderate compound increases or severe, persistent compound stress. Consequently, temperature-centric risk frameworks alone are insufficient for capturing compound vulnerability patterns across Africa.

Despite projected increases in precipitation across much of tropical Africa, compound hot–dry extremes intensify in all regions by the end of the century. Even relatively protected regions, such as West Africa, experience compound frequency increases from approximately 0.08–0.15 months yr^{-1} at mid-century to 0.11–0.22 months yr^{-1} by 2070–2100 under high emissions. This universal increase underscores that no African region is fully insulated from compound climate risk, even where mean precipitation increases. In hyper-arid environments such as the Sahara, extreme warming alone is sufficient to drive frequent compound conditions despite modest wetting, illustrating that mean precipitation trends cannot be interpreted in isolation.

The inter-scenario spread in compound risk quantifies the substantial mitigation benefit for Africa. Under aggressive mitigation consistent with the Paris Agreement (RCP2.6/SSP1-2.6), late-century compound frequencies remain below ~0.3 months yr^{-1} across most regions, mean event durations remain near 2 months, and magnitudes remain moderate. Under continued high emissions (RCP8.5/SSP5-8.5), frequencies rise to 0.4–0.6 months yr^{-1} in vulnerable regions, durations extend to 4–6 months, and magnitudes reach 10–13σ—representing a doubling to

https://doi.org/10.5194/egusphere-2026-721
Preprint. Discussion started: 10 March 2026
© Author(s) 2026. CC BY 4.0 License.

tripling of compound risk attributable solely to emission pathway choice. These differences highlight that mitigation not only limits warming but also constrains the nonlinear land–atmosphere feedbacks that amplify compound extremes.

From an adaptation perspective, our findings emphasize the need for compound-aware climate risk frameworks. Adaptation strategies must be regionally differentiated based on precipitation trajectories rather than uniform warming assumptions. Southern African regions require integrated approaches addressing chronic water scarcity and extreme heat simultaneously, while northeastern Africa may focus on managing increased precipitation variability alongside reduced compound drought–heat risk. Moreover, the projected extension of compound event duration necessitates reconsidering agricultural calendars, reservoir operation rules, ecosystem management strategies, and social protection systems, which are currently calibrated to short-lived extremes.

Several limitations are acknowledged. Multi-model ensemble means mask inter-model spread, particularly for precipitation projections, and observational uncertainties persist in data-sparse regions. Additionally, fixed percentile thresholds do not capture potential shifts in impact-relevant thresholds as the climate warms. Future work may incorporate large ensembles, higher-resolution regional modeling, and sector-specific impact thresholds to refine compound risk estimates.

Compound hot–dry extremes across Africa will intensify irrespective of mean precipitation trends, driven by accelerated warming and modulated by regionally divergent moisture responses. The combined increase in frequency, magnitude, and duration signals a transition toward more persistent and severe compound stress, particularly in southern Africa and Madagascar. These results underscore the urgency of compound-aware adaptation strategies and demonstrate the substantial benefits of mitigation for limiting future climate impacts on a continent uniquely vulnerable to concurrent heat and drought stress.

Authors contribution

PA: Writing – review & editing, Writing –original draft, Formal analysis, Data curation, Conceptualization, Visualization, and Validation. ATO: Writing – review & editing, Funding acquisition. KD and XX: Supervision, Project administration, Writing – review & editing. EP, MUN, and ESB: Writing – review & editing.

Declaration of competing interest

The authors declare that they have no known competing financial interests or personal relationships that could have appeared to influence the work reported in this paper.

https://doi.org/10.5194/egusphere-2026-721
Preprint. Discussion started: 10 March 2026
© Author(s) 2026. CC BY 4.0 License.

Availability of data and material

The CMIP6 data is available from the Earth System Grid Federation (ESGF) repository (https://esgf-node.llnl.gov/projects/cmip6/). The CMIP5 data is available from the Earth System Grid Federation (ESGF) repository (https://esgf-node.llnl.gov/projects/cmip5/). The CRU TS4.08 data is available from the Centre for Environmental Data Analysis (CEDA) repository (https://crudata.uea.ac.uk/cru/data/hrg/cru_ts_4.08/).

Code availability

The Python scripts utilized in the analysis are accessible upon reasonable request.

Funding

The study was supported by the Northwest Institute of Ecological Environment and Resources, Chinese Academy of Science (grant number: E429020101).

References

AghaKouchak, A., Chiang, F., Huning, L. S., Love, C. A., Mallakpour, I., Mazdiyasni, O., Moftakhari, H., Papalexiou, S. M., Ragno, E., & Sadegh, M. (2020). Climate extremes and compound hazards in a warming world. *Annual Review of Earth and Planetary Sciences*, 48, 519-546. https://doi.org/10.1146/annurev-earth-071719-055228

Almazroui, M., Saeed, F., Saeed, S., Nazrul Islam, M., Ismail, M., Klutse, N. A. B., & Siddiqui, M. H. (2020). Projected change in temperature and precipitation over Africa from CMIP6. *Earth Systems and Environment*, 4(3), 455-475. https://doi.org/10.1007/s41748-020-00161-x

Archer, E. R. M., Landman, W. A., Tadross, M. A., Malherbe, J., Weepener, H., Maluleke, P., & Marumbwa, F. M. (2021). The 2015-19 multi year drought in the Eastern Cape, South Africa: it's evolution and impacts on agriculture. *Journal of Arid Environments*, 194, 104368. https://doi.org/10.1016/j.jaridenv.2021.104630

Bevacqua, E., Suarez-Gutierrez, L., Jézéquel, A., Lehner, F., Vrac, M., Yiou, P., & Zscheischler, J. (2023). Advancing research on compound weather and climate events via large ensemble model simulations. Nature Communications, 14(1), 2145. https://doi.org/10.1038/s41467-023-37847-5

Berg, A., & Sheffield, J. (2018). Soil moisture–evapotranspiration coupling in CMIP5 models: Relationship with simulated climate and projections. *Journal of Climate*, 31(12), 4865-4878. https://doi.org/10.1175/JCLI-D-17-0757.1

Clement, V., Rigaud, K. K., De Sherbinin, A., Jones, B., Adamo, S., Schewe, J., ... & Shabahat, E. (2021). Groundswell part 2: Acting on internal climate migration.

https://doi.org/10.5194/egusphere-2026-721
Preprint. Discussion started: 10 March 2026
© Author(s) 2026. CC BY 4.0 License.

Chou, C., Neelin, J. D., Chen, C. A., & Tu, J. Y. (2009). Evaluating the "rich-get-richer" mechanism in tropical precipitation change under global warming. *Journal of Climate*, 22(8), 1982-2005. https://doi.org/10.1175/2008JCLI2471.1

Collins, M. (2011). Temperature variability over Africa. *Journal of Climate*, 24(14), 3649-3666. https://doi.org/10.1175/2011JCLI3753.1

Creese, A., & Washington, R. (2016). Using qflux to constrain modeled Congo Basin rainfall in the CMIP5 ensemble. *Journal of Geophysical Research: Atmospheres*, 121(22), 13,415-13,442. https://doi.org/10.1002/2016JD025596

Dosio, A., Jury, M. W., Almazroui, M., Ashfaq, M., Diallo, I., Engelbrecht, F. A., ... & Tamoffo, A. T. (2021). Projected future daily characteristics of African precipitation based on global (CMIP5, CMIP6) and regional (CORDEX, CORDEX-CORE) climate models. Climate Dynamics, 57(11), 3135-3158. https://doi.org/10.1007/s00382-021-05859-w

Engelbrecht, F., Adegoke, J., Bopape, M. J., Naidoo, M., Garland, R., Thatcher, M., McGregor, J., Katzfey, J., Werner, M., Ichoku, C., & Gatebe, C. (2015). Projections of rapidly rising surface temperatures over Africa under low mitigation. *Environmental Research Letters*, 10(8), 085004. https://doi.org/10.1088/1748-9326/10/8/085004

Eyring, V., Bony, S., Meehl, G. A., Senior, C. A., Stevens, B., Stouffer, R. J., & Taylor, K. E. (2016). Overview of the Coupled Model Intercomparison Project Phase 6 (CMIP6) experimental design and organization. Geoscientific Model Development, 9(5), 1937-1958. https://doi.org/10.5194/gmd-9-1937-2016

Liebmann, B., Bladé, I., Kiladis, G. N., Carvalho, L. M., B. Senay, G., Allured, D., ... & Funk, C. (2012). Seasonality of African precipitation from 1996 to 2009. *Journal of Climate*, *25*(12), 4304-4322. *Journal of Climate*, 25(12), 4304-4322. https://doi.org/10.1175/JCLI-D-11-00157.1

Gebrechorkos, S. H., Hülsmann, S., & Bernhofer, C. (2019). Long-term trends in rainfall and temperature using high-resolution climate datasets in East Africa. *Scientific Reports*, 9(1), 11376. https://doi.org/10.1038/s41598-019-47933-8

Gutiérrez, J. M., Jones, R. G., Narisma, G. T., Alves, L. M., Amjad, M., Gorodetskaya, I. V., Grose, M., Klutse, N. A. B., Krakovska, S., Li, J., Martínez-Castro, D., Mearns, L. O., Mernild, S. H., Ngo-Duc, T., van den Hurk, B., & Yoon, J. H. (2021). Atlas. In *Climate Change 2021: The Physical Science Basis. Contribution of Working Group I to the Sixth Assessment Report of the Intergovernmental Panel on Climate Change*. Cambridge University Press, 1927-2058. https://doi.org/10.1017/9781009157896.021

Hagemann, S., Chen, C., Clark, D. B., Folwell, S., Gosling, S. N., Haddeland, I., Hanasaki, N., Heinke, J., Ludwig, F., Voss, F., & Wiltshire, A. (2013). Climate change impact on available water

https://doi.org/10.5194/egusphere-2026-721
Preprint. Discussion started: 10 March 2026
© Author(s) 2026. CC BY 4.0 License.

resources obtained using multiple global climate and hydrology models. *Earth System Dynamics*, 4(1), 129-144. https://doi.org/10.5194/esd-4-129-2013

Harris, I., Osborn, T. J., Jones, P., & Lister, D. (2020). Version 4 of the CRU TS monthly high-resolution gridded multivariate climate dataset. *Scientific Data*, 7(1), 109. https://doi.org/10.1038/s41597-020-0453-3

Hirschi, M., Seneviratne, S. I., Alexandrov, V., Boberg, F., Boroneant, C., Christensen, O. B., Formayer, H., Orlowsky, B., & Stepanek, P. (2011). Observational evidence for soil-moisture impact on hot extremes in southeastern Europe. *Nature Geoscience*, 4(1), 17-21. https://doi.org/10.1038/ngeo1032

IPCC. (2021). *Climate Change 2021: The Physical Science Basis. Contribution of Working Group I to the Sixth Assessment Report of the Intergovernmental Panel on Climate Change*. Cambridge University Press. https://doi.org/10.1017/9781009157896

Iturbide, M., Gutiérrez, J. M., Alves, L. M., Bedia, J., Cerezo-Mota, R., Cimadevilla, E., Cofiño, A. S., Di Luca, A., Faria, S. H., Gorodetskaya, I. V., Hauser, M., Herrera, S., Hennessy, K., Hewitt, H. T., Jones, R. G., Krakovska, S., Manzanas, R., Martínez-Castro, D., Narisma, G. T., Nurhati, I. S., Pinto, I., Seneviratne, S. I., van den Hurk, B., & Vera, C. S. (2020). An update of IPCC climate reference regions for subcontinental analysis of climate model data: definition and aggregated datasets. *Earth System Science Data*, 12(4), 2959-2970. https://doi.org/10.5194/essd-12-2959-2020

Lesk, C., Rowhani, P., & Ramankutty, N. (2016). Influence of extreme weather disasters on global crop production. *Nature*, 529(7584), 84-87. https://doi.org/10.1038/nature16467

Lyon, B., & DeWitt, D. G. (2012). A recent and abrupt decline in the East African long rains. *Geophysical Research Letters*, 39(2), L02702. https://doi.org/10.1029/2011GL050337

Manning, C., Widmann, M., Bevacqua, E., Van Loon, A. F., Maraun, D., & Vrac, M. (2019). Increased probability of compound long-duration dry and hot events in Europe during summer (1950–2013). *Environmental Research Letters*, *14*(9), 094006. https://doi.org/10.1088/1748-9326/ab23bf

Martens, B., Miralles, D. G., Lievens, H., Van Der Schalie, R., De Jeu, R. A., Fernández-Prieto, D., ... & Verhoest, N. E. (2017). GLEAM v3: Satellite-based land evaporation and root-zone soil moisture. *Geoscientific Model Development*, *10*(5), 1903-1925. https://doi.org/10.5194/gmd-10-1903-2017

Maúre, G., Pinto, I., Ndebele-Murisa, M., Muthige, M., Lennard, C., Nikulin, G., Dosio, A., & Meque, A. (2018). The southern African climate under 1.5 °C and 2 °C of global warming as

https://doi.org/10.5194/egusphere-2026-721
Preprint. Discussion started: 10 March 2026
© Author(s) 2026. CC BY 4.0 License.

simulated by CORDEX regional climate models. *Environmental Research Letters*, 13(6), 065002. https://doi.org/10.1088/1748-9326/aab190

Meehl, G. A., Senior, C. A., Eyring, V., Flato, G., Lamarque, J. F., Stouffer, R. J., Taylor, K. E., & Schlund, M. (2020). Context for interpreting equilibrium climate sensitivity and transient climate response from the CMIP6 Earth system models. *Science Advances*, 6(26), eaba1981. https://doi.org/10.1126/sciadv.aba1981

Miralles, D. G., Gentine, P., Seneviratne, S. I., & Teuling, A. J. (2019). Land–atmospheric feedbacks during droughts and heatwaves: state of the science and current challenges. *Annals of the New York Academy of Sciences*, *1436*(1), 19-35.. https://doi.org/10.1111/nyas.13912

Munday, C., & Washington, R. (2018). Systematic climate model rainfall biases over southern Africa: Links to moisture circulation and topography. *Journal of Climate*, *31*(18), 7533-7548. https://doi.org/10.1175/JCLI-D-18-0008.1

Nicholson, S. E. (2013). The West African Sahel: A review of recent studies on the rainfall regime and its interannual variability. *International Scholarly Research Notices*, 2013, 453521. https://doi.org/10.1155/2013/453521

O'Neill, B. C., Kriegler, E., Ebi, K. L., Kemp-Benedict, E., Riahi, K., Rothman, D. S., ... & Solecki, W. (2017). The roads ahead: Narratives for shared socioeconomic pathways describing world futures in the 21st century. Global environmental change, 42, 169-180. https://doi.org/10.1016/j.gloenvcha.2015.01.004

Ongoma, V., & Chen, H. (2017). Temporal and spatial variability of temperature and precipitation over East Africa from 1951 to 2010. *Meteorology and Atmospheric Physics*, *129*(2), 131-144. https://doi.org/10.1007/s00703-016-0462-0.

Riahi, K., van Vuuren, D. P., Kriegler, E., Edmonds, J., O'Neill, B. C., Fujimori, S., Bauer, N., Calvin, K., Dellink, R., Fricko, O., Lutz, W., Popp, A., Cuaresma, J. C., KC, S., Leimbach, M., Jiang, L., Kram, T., Rao, S., Emmerling, J., Ebi, K., Hasegawa, T., Havlik, P., Humpenöder, F., Da Silva, L. A., Smith, S., Stehfest, E., Bosetti, V., Eom, J., Gernaat, D., Masui, T., Rogelj, J., Strefler, J., Drouet, L., Krey, V., Luderer, G., Harmsen, M., Takahashi, K., Baumstark, L., Doelman, J. C., Kainuma, M., Klimont, Z., Marangoni, G., Lotze-Campen, H., Obersteiner, M., Tabeau, A., & Tavoni, M. (2017). The Shared Socioeconomic Pathways and their energy, land use, and greenhouse gas emissions implications: An overview. *Global Environmental Change*, 42, 153-168. https://doi.org/10.1016/j.gloenvcha.2016.05.009

Rowell, D. P., Booth, B. B. B., Nicholson, S. E., & Good, P. (2015). Reconciling past and future rainfall trends over East Africa. *Journal of Climate*, 28(24), 9768-9788. https://doi.org/10.1175/JCLI-D-15-0140.1

https://doi.org/10.5194/egusphere-2026-721
Preprint. Discussion started: 10 March 2026
© Author(s) 2026. CC BY 4.0 License.

Schewe, J., Heinke, J., Gerten, D., Haddeland, I., Arnell, N. W., Clark, D. B., Dankers, R., Eisner, S., Fekete, B. M., Colón-González, F. J., Gosling, S. N., Kim, H., Liu, X., Masaki, Y., Portmann, F. T., Satoh, Y., Stacke, T., Tang, Q., Wada, Y., Wisser, D., Albrecht, T., Frieler, K., Piontek, F., Warszawski, L., & Kabat, P. (2014). Multimodel assessment of water scarcity under climate change. *Proceedings of the National Academy of Sciences*, 111(9), 3245-3250. https://doi.org/10.1073/pnas.1222460110

Seneviratne, S. I., Corti, T., Davin, E. L., Hirschi, M., Jaeger, E. B., Lehner, I., Orlowsky, B., & Teuling, A. J. (2010). Investigating soil moisture–climate interactions in a changing climate: A review. *Earth-Science Reviews*, 99(3-4), 125-161. https://doi.org/10.1016/j.earscirev.2010.02.004

Seneviratne, S. I., Zhang, X., Adnan, M., Badi, W., Dereczynski, C., Di Luca, A., Ghosh, S., Iskandar, I., Kossin, J., Lewis, S., Otto, F., Pinto, I., Satoh, M., Vicente-Serrano, S. M., Wehner, M., & Zhou, B. (2021). Weather and climate extreme events in a changing climate. In *Climate Change 2021: The Physical Science Basis. Contribution of Working Group I to the Sixth Assessment Report of the Intergovernmental Panel on Climate Change*. Cambridge University Press, 1513-1766. https://doi.org/10.1017/9781009157896.013

Sultan, B., & Gaetani, M. (2016). Agriculture in West Africa in the twenty-first century: Climate change and impacts scenarios, and potential for adaptation. *Frontiers in Plant Science*, 7, 1262. https://doi.org/10.3389/fpls.2016.01262

Taylor, K. E., Stouffer, R. J., & Meehl, G. A. (2012). An overview of CMIP5 and the experiment design. *Bulletin of the American Meteorological Society*, 93(4), 485-498. https://doi.org/10.1175/BAMS-D-11-00094.1

Thornton, P. K., Jones, P. G., Ericksen, P. J., & Challinor, A. J. (2011). Agriculture and food systems in sub-Saharan Africa in a 4°C+ world. *Philosophical Transactions of the Royal Society A: Mathematical, Physical and Engineering Sciences*, 369(1934), 117-136. https://doi.org/10.1098/rsta.2010.0246

Trenberth, K. E., & Shea, D. J. (2005). Relationships between precipitation and surface temperature. *Geophysical Research Letters*, 32(14), L14703. https://doi.org/10.1029/2005GL022760

Trisos, C. H., Adelekan, I. O., Totin, E., Ayanlade, A., Efitre, J., Gemeda, A., Kalaba, K., Lennard, C., Masao, C., Mgaya, Y., Ngaruiya, G., Olago, D., Simpson, N. P., & Zakieldeen, S. (2022). Africa. In *Climate Change 2022: Impacts, Adaptation and Vulnerability. Contribution of Working Group II to the Sixth Assessment Report of the Intergovernmental Panel on Climate Change*. Cambridge University Press, 1285-1455. https://doi.org/10.1017/9781009325844.011

https://doi.org/10.5194/egusphere-2026-721
Preprint. Discussion started: 10 March 2026
© Author(s) 2026. CC BY 4.0 License.

UNFCCC. (2015). *Paris Agreement*. United Nations Framework Convention on Climate Change. https://unfccc.int/files/meetings/paris_nov_2015/application/pdf/paris_agreement_english_.pdf

van Vuuren, D. P., Edmonds, J., Kainuma, M., Riahi, K., Thomson, A., Hibbard, K., Hurtt, G. C., Kram, T., Krey, V., Lamarque, J. F., Masui, T., Meinshausen, M., Nakicenovic, N., Smith, S. J., & Rose, S. K. (2011). The representative concentration pathways: an overview. *Climatic Change*, 109(1-2), 5-31. https://doi.org/10.1007/s10584-011-0148-z

Vogel, M. M., Zscheischler, J., Wartenburger, R., Dee, D., & Seneviratne, S. I. (2021). Concurrent 2018 hot extremes across Northern Hemisphere due to human-induced climate change. *Earth's Future*, 7(7), 692-703. https://doi.org/10.1029/2019EF001189

Warszawski, L., Frieler, K., Huber, V., Piontek, F., Serdeczny, O., & Schewe, J. (2014). The Inter-Sectoral Impact Model Intercomparison Project (ISI–MIP): Project framework. *Proceedings of the National Academy of Sciences*, 111(9), 3228-3232. https://doi.org/10.1073/pnas.1312330110

WMO. (2017). *WMO Guidelines on the Calculation of Climate Normals*. World Meteorological Organization. https://library.wmo.int/doc_num.php?explnum_id=4166

Zelinka, M. D., Myers, T. A., McCoy, D. T., Po-Chedley, S., Caldwell, P. M., Ceppi, P., ... & Taylor, K. E. (2020). Causes of higher climate sensitivity in CMIP6 models. *Geophysical Research Letters*, *47*(1), e2019GL085782. https://doi.org/10.1029/2019GL085782

Zhou, S., Williams, A. P., Berg, A. M., Cook, B. I., Zhang, Y., Hagemann, S., Lorenz, R., Seneviratne, S. I., & Gentine, P. (2019). Land–atmosphere feedbacks exacerbate concurrent soil drought and atmospheric aridity. *Proceedings of the National Academy of Sciences*, 116(38), 18848-18853. https://doi.org/10.1073/pnas.1904955116

Zscheischler, J., Westra, S., van den Hurk, B. J. J. M., Seneviratne, S. I., Ward, P. J., Pitman, A., AghaKouchak, A., Bresch, D. N., Leonard, M., Wahl, T., & Zhang, X. (2018). Future climate risk from compound events. *Nature Climate Change*, 8(6), 469-477. https://doi.org/10.1038/s41558-018-0156-3

Zscheischler, J., Martius, O., Westra, S., Bevacqua, E., Raymond, C., Horton, R. M., van den Hurk, B., AghaKouchak, A., Jézéquel, A., Mahecha, M. D., Maraun, D., Ramos, A. M., Ridder, N. N., Thiery, W., & Vignotto, E. (2020). A typology of compound weather and climate events. *Nature Reviews Earth & Environment*, 1(7), 333-347. https://doi.org/10.1038/s43017-020-0060-z

Zscheischler, J., & Seneviratne, S. I. (2017). Dependence of drivers affects risks associated with compound events. *Science Advances*, 3(6), e1700263. https://doi.org/10.1126/sciadv.1700263